Monthly Notices of the ROYAL ASTRONOMICAL SOCIETY

MNRAS **518,** 6223–6237 (2023) https://doi.org/10.1093/mnras/stac3488
Advance Access publication 2022 November 28

Hyper-runaway and hypervelocity white dwarf candidates in *Gaia* Data Release 3: Possible remnants from Ia/Iax supernova explosions or dynamical encounters

Andrei P. Igoshev [1]★ Hagai Perets [2] and Na'ama Hallakoun [3]

[1]*Department of Applied Mathematics, University of Leeds, LS2 9JT Leeds, UK*
[2]*Physics Department, Technion - Israel Institute of Technology, Haifa 3200002, Israel*
[3]*Department of particle physics and astrophysics, Weizmann Institute of Science, Rehovot 7610001, Israel*

Accepted 2022 November 24. Received 2022 November 16; in original form 2022 September 18

ABSTRACT

Type Ia and other peculiar supernovae (SNe) are thought to originate from the thermonuclear explosions of white dwarfs (WDs). Some of the proposed channels involve the ejection of a partly exploded WD (e.g. Iax SN remnant) or the companion of an exploding WD at extremely high velocities ($>400\,\mathrm{km\,s^{-1}}$). Characterization of such hyper-runaway/hypervelocity (HVS) WDs might therefore shed light on the physics and origins of SNe. Here we analyse the *Gaia* DR3 data to search for HVS WDs candidates and peculiar sub-main-sequence (sub-MS) objects. We retrieve the previously identified HVSs and find 46 new HVS candidates. Among these we identify two new unbound WDs and two new unbound sub-MS candidates. The remaining stars are hyper-runaway WDs and hyper-runaway sub-MS stars. The numbers and properties of the HVS WD and sub-MS candidates suggest that extreme velocity ejections ($>1000\,\mathrm{km\,s^{-1}}$) can accompany at most a small fraction of type Ia SNe, disfavouring a significant contribution of the D6-scenario to the origin of Ia SNe. The rate of HVS ejections following the hybrid WD reverse-detonation channel could be consistent with the identified HVSs. The numbers of lower-velocity HVS WDs could be consistent with type Iax SNe origin and/or contribution from dynamical encounters. We also searched for HVS WDs related to known SN remnants but identified only one such candidate.

Key words: methods: statistical – subdwarfs – supernovae: general – white dwarfs.

1 INTRODUCTION

Most stars in the Galaxy reside in the Galactic disc, and have low peculiar velocities. The typical velocity dispersion of stars in the disc is of a few tens of $\mathrm{km\,s^{-1}}$. However, a small fraction of stars and compact objects are known to have far higher velocities of hundreds and even thousands of $\mathrm{km\,s^{-1}}$ with respect to local standard of rest (LSR) and could even be unbound to the Galaxy. Such Galactic hyper-runaway and hypervelocity (HVS) stars and compact objects have been studied for decades, as the origin of their high peculiar velocities provides potential input on the physical processes which have accelerated these stars. These include stellar evolutionary processes, such as natal kicks given to neutron stars (NS) (Lyne & Lorimer 1994; Arzoumanian, Chernoff & Cordes 2002; Verbunt, Igoshev & Cator 2017; Igoshev 2020) and possibly other type of compact objects (Repetto, Davies & Sigurdsson 2012; Repetto, Igoshev & Nelemans 2017; El-Badry & Rix 2018); binary evolution processes, such as supernova kicks in binaries (Brandt & Podsiadlowski 1995; Igoshev et al. 2021), ejecting the companion of the exploding stars at velocities comparable to the orbital velocities at the point of the explosion (Blaauw 1961; Hoogerwerf, de Bruijne & de Zeeuw 2001; Eldridge, Langer & Tout 2011; Renzo et al. 2019), remnants of Ia/Iax supernova explosion; and stellar dynamical processes in collisional cluster environments, where few-body interactions can give rise to hyper-runaway ejections; or through dynamical interactions with massive black holes that may even give rise to extreme HVS stars ejected at hundreds or thousands of $\mathrm{km\,s^{-1}}$ (Hills 1988).

One of the most intriguing aspects of the study of hyper-runaway stars is their potential use in constraining and characterizing the still highly debated origins of type I (and in particular type Ia) supernovae (SNe) originating from thermonuclear explosions of white dwarfs (WDs). Different suggested models for normal and peculiar types of such SNe pointed to various channels for the ejection of hyper-runaway WDs, with distinct predictions. Identifying and characterizing the properties, rates and distributions of such WDs can therefore shed light on the origins of thermonuclear SNe.

WDs are formed following the evolution of stars with up to 8–10 $\mathrm{M_\odot}$ and typically above 0.8–0.9 $\mathrm{M_\odot}$. More massive stars explode as core-collapse SNe and form NS or black holes, while lower-mass stars do not evolve to become WDs during Hubble time. This is true for single stars, while the evolution of stars in interacting binaries could be somewhat altered by mass-transfer and/or stripping.

In order to put our work in the context we briefly summarize here different scenarios for SNe Ia/Iax and their rates and expected observational outcomes. At the end of the article, we compare these rates with number of hyper-runaway WD candidates found in the *Gaia* data base.

★ E-mails: ignotur@gmail.com, a.igoshev@leeds.ac.uk

The double degenerate dynamical detonations scenario was suggested by Guillochon et al. (2010), Fink et al. (2010). In this scenario two CO WDs with thin surface helium layers remaining from single stellar evolution can lead to a SNe Ia (this scenario is sometimes called the dynamically driven double-degenerate double-detonation, or D6, scenario Shen et al. 2018). After the progenitor stars evolve through single stellar and common-envelope evolution, they eventually form a compact WD–WD binary, whose components are then driven towards increasingly shorter periods by gravitational wave-driven inspiral. The Roche lobe overflow of the donor then provides a helium-rich accretion stream on to the companion. The dynamically formed He layer and its accretion heat the He surface layer which then experiences a thermonuclear detonation (Guillochon et al. 2010). The convergence of the detonation front was suggested to give rise to a second detonation inside the accretor's CO core. This second detonation in the CO core disrupts the accretor and gives rise to a type Ia event.[1] The proposed D6 scenario therefore differs from the classic double degenerate scenario in a crucial respect: the donor WD survives the SN Ia event. Specifically, in the D6 scenario, the WD donor is ejected after the detonation of the accretor, at the Keplerian velocity at the point of Roche lobe overflow, a speed of several thousand $\mathrm{km\,s^{-1}}$ and generally above $1000\,\mathrm{km\,s^{-1}}$.

The hybrid-WD reverse detonation scenario was suggested by Pakmor et al. (2021). In this scenario a highly He enriched hybrid HeCO-WD begins transferring mass on to a more massive CO-WD companion, similar to the D6 model mentioned above, leading to a He surface detonation of the CO WD. However, the He surface detonation fails to induce a detonation in the CO WD, and instead, the nuclear burning front propagates back to the donor hybrid HeCO WD, and the shock leads to its core detonation and disruption, which leaves the primary CO WD intact. The leftover primary WD is ejected at high velocity, comparable with its Keplerian orbital velocity at the time. Like the D6 scenario, the origin of the velocity excitation is the Keplerian motion in the compact binary at the time of the explosion. In this case, it is the secondary, less massive WD which is disrupted, and therefore the typical ejection velocities of the primary are somewhat lower than the D6 case, typically between 1000–$1500\,\mathrm{km\,s^{-1}}$. The ejected WD might be somewhat heated from the surface detonation and polluted by the companion ejecta, but likely not very significantly. The expected ejection rates are of the order of 1 per cent of the Ia SNe rate (Pakmor et al. 2021).

The failed-detonation or weak deflagration model for SNe Iax was suggested by one of us (Jordan et al. 2012). In this scenario, it is suggested that a CO WD accretes mass from a companion at an appropriate rate that allows it to accumulate mass and eventually reach close to Chandrasekhar mass, at which point it detonates producing a SN. In Jordan et al. (2012) (see also Kromer et al. 2013), one of us studied the last stages of the evolution of a near-Chandrasekhar CO WD and suggested that ignition of nuclear burning might not lead to a full detonation but may only give rise to a weak asymmetric deflagration, which would then partially burn some of the WD and eject some of its mass, leading to the production of faint peculiar Ia SNe, which we proposed could explain the origin of type Iax SNe. The weak explosion should leave a somewhat lower mass, likely very hot WD (due to burning and ejection of up to a few $0.1\,\mathrm{M_\odot}$ of material) but otherwise intact and polluted with heavier burning product elements. Such an asymmetric explosion would likely also eject the WD at high velocities of hundreds of $\mathrm{km\,s^{-1}}$ possibly up to $500\,\mathrm{km\,s^{-1}}$ in the most extreme case modelled. We therefore, suggested searching for hyper-runaway WDs with peculiar properties, likely being massive, hot and showing significant pollution by intermediate and iron elements. The inferred rate of type Iax SNe is of the order of 20–50 per cent of the type Ia SNe rate (Foley et al. 2013) if ultra-faint 2008ha-like SNe is included. The rate is likely lower, of the order of 2–10 per cent, if only brighter 2002cx-like SNe are considered as part of this class (Li et al. 2011).

Single-degenerate double-detonation scenario was suggested by Woosley et al. (1986). In this scenario, it was suggested that a sufficiently massive WD can accrete and accumulate He from a stripped He-rich stellar companion, which becomes an sdB/O star. After a critical mass is deposited on the surface of the WD, a surface helium ignition may occur, which then triggers the explosion of the CO core of the WD (Woosley et al. 1986). Like in the D6 and reverse-detonation scenarios discussed above, the disruption of the exploding WD unbinds the companion which is therefore ejected at velocities comparable to its orbital velocity in the progenitor binary. Unlike the previous channels mentioned above, the companion in this case is a sdB/O star whose size and Roche radius are larger than that of a WD and therefore the orbit of the progenitor binary of the system cannot be as close as that of a double-WD system. Geier et al. (2015) suggested that US-708 could be explained by such a scenario and suggested ejection at velocities exceeding $1000\,\mathrm{km\,s^{-1}}$, however Liu et al. (2021) showed in a detailed study that in the relevant case, one can at most achieve $600\,\mathrm{km\,s^{-1}}$. More generally, although under extreme conditions one might get very high velocities, in most cases the ejection velocities are limited to a lower range of a few hundred $\mathrm{km\,s^{-1}}$ (Meng & Luo 2021). It is therefore possible that this scenario can explain hyper-runaway sdB/O (which would later evolve to become hyper-runaway WDs). Neunteufel et al. (2022) used population synthesis studies and suggested that the theoretical ejection rate of unbound He-rich stars through this mechanism is two orders of magnitude higher than expected given the single identification of US-708 possibly ruling out this scenario.

Beside these scenarios, the hyper-runaway WD could also be ejected dynamically from globular clusters and Milky Way centre. Some of these WDs could have been stripped from inspiraling galaxies. Some other WD could in fact be members of binaries and received their large speed due to supernova explosion. We consider these alternative routes in more details in the Discussion section.

The discovery of three HVS[2] WDs in the *Gaia* DR2 catalogue provided potential observational evidence of the ex-companions of sub-Chandrasekhar WDs which underwent SNe Ia explosions in a dynamical detonation variant of the double-degenerate scenario (Shen et al. 2018).

O and B stars are known to have a non-negligible fraction of runaway stars, i.e. stars observed to have particularly high peculiar velocities of above 30–40 $\mathrm{km\,s^{-1}}$, significantly larger than their expected initial velocities at birth (Hoogerwerf et al. 2001; Eldridge et al. 2011; Renzo et al. 2019). WDs which originate from B-stars could therefore posses such high peculiar velocities. The dynamical

[1] If the second detonation does not occur, only the first weak explosion occurs, likely leading to a peculiar SN Woosley, Taam & Weaver (1986), Bildsten et al. (2007). In Perets et al. (2010) and Zenati et al. (2022) we suggested and showed that these could be the progenitors of Ca-rich SNe the primary is a hybrid HeCO WD. In this case, the companion is disrupted and not ejected as a hyper-runaway WD. Whether the remnant from the primary can be ejected is not clear and likely require 3D models to explore whether an asymmetric explosion occurs and give rise to the ejection of the partially burned primary.

[2] We adopted the following notation throughout the manuscript. We call a star HVS if it is unbound from the Galaxy. The hyper-runaway star has velocity above our minimum velocity threshold.

perturbation by massive perturbers, such as giant molecular clouds and stellar clusters, as well as spiral arms in the Galactic disc can excite the stellar velocities over time, and, thereby older stellar populations show higher velocity dispersions. In particular, WDs formed in the disc, whose age can extend up to the age of the Galaxy, could belong to the oldest populations and have tens of $\mathrm{km\,s^{-1}}$ peculiar velocities. A small fraction of them might also be part of the Galactic halo, where the velocity dispersion is far greater and can reach hundreds of $\mathrm{km\,s^{-1}}$ up to the Galactic escape velocity.

Here we focus on the hyper-runaway/HVS WD regime, at velocities of hundreds of $\mathrm{km\,s^{-1}}$ or above, which are unlikely to be produced through stellar evolution or through most of the dynamical processes discussed above but could be the result of thermonuclear explosions such as the D6, and the reverse hybrid detonation of failed deflagration/detonation scenarios.

We therefore focus on WDs with extreme velocities of typically $>500\,\mathrm{km\,s^{-1}}$, much higher than the velocity dispersion of disc stars and potentially higher than the Galactic escape velocity. However, since in most cases only data for the tangential velocity are known, we identify the fastest 1000 objects, which effectively give us a lower velocity limit of $400\,\mathrm{km\,s^{-1}}$ for the 2D velocities throughout this study. This less conservative cut is made in order to avoid missing potential HVS WD candidates, as well as to find potential candidates produced in failed detonation/deflagration. In addition, we also identify other peculiar candidate hyper-runaways and HVS objects which reside above the WD cooling sequence but significantly below the MS. Since WD remnants of SNe might be heated or affected by the explosion, they might not resemble normal WDs, and therefore a complementary search for such 'peculiar' objects is also presented here. In particular, the objects DR61–DR6-3 (identified by Shen et al. 2018) are not located in the expected region of the WDs and are not considered to be WDs in our initial criteria, as we discuss below.

Our paper is structured as the following: in Section 2, we summarize the information about known HVS candidates; in Section 3, we describe our selection procedure and summarize new candidates. In Section 4, we list and discuss the observational properties of our main candidates. In Section 5, we look for potential associations between our HVS WDs and supernova remnants (SNR). In Section 6, we list and discuss all potential scenarios to produce HVS WDs and sdBs.

2 PREVIOUSLY CHARACTERIZED HVS WD CANDIDATES

Here we discuss the detailed properties of the selected objects, found through a literature search and/or other archival observations. Some of these are further discussed later on, in the context of our analysis and the distribution of the candidate samples.

(i) **LSPM J1852+6202**, ***Gaia*** **EDR3 5805243926609660032** and **LP 398-9** were identified as HVS WD candidates by Shen et al. (2018). These are their candidate D6-3, D6-1, and D6-2, respectively. Scholz (2018a), taking a higher tangential velocity cutoff, considered only D6-2 to be a HVS star. Scholz (2018a) suggested that even this candidate is suspicious because of its relatively poor astrometric quality parameters. Moreover, the low radial velocities of D6-2 and D6-3 also cast doubt on the nature of these candidates being bona fide HVS WDs. The radial velocity of D6-1 is $1200 \pm 40\,\mathrm{km\,s^{-1}}$ (Shen et al. 2018).

(ii) **LP40-365** also known as GD 492 is a high proper motion WD with peculiar chemical composition (Raddi et al. 2018a,b) dominated by intermediate-mass elements. It was suggested as remnant of Iax supernova by Vennes et al. (2017). This WD has high tangential velocity of $497.6 \pm 1.1\,\mathrm{km\,s^{-1}}$ (Vennes et al. 2017). This WD is slowly rotating with spin period of 8.914 h (Hermes et al. 2021). We identified LP 40-365 among our sub-MS stars, but we did not include it into our final selection because it has a nominal 2D velocity of $454\,\mathrm{km\,s^{-1}}$ (below sub-MS cut of $550\,\mathrm{km\,s^{-1}}$), nevertheless this velocity is consistent with a Iax remnant and omitted only due our focus on even higher velocity objects. Raddi et al. (2019) discovered three more chemically peculiar, runaway stars. These are stars J1603-6613 (also known as *Gaia* DR2 5822236741381879040), J1825-3757 (also known as *Gaia* DR2 6727110900983876096), and J0905+2510 (also known as *Gaia* DR2 688380457507044864). These have Ne dominated atmospheres with presence of O and Mg, low masses ($\approx 0.2\,\mathrm{M_\odot}$) and ejection velocities around 550–$600\,\mathrm{km\,s^{-1}}$. The star J1825-3757 is found in our extended search.

(iii) **LP91-84** is a hot subdwarf which is included in a survey of large proper motion stars (Lépine & Shara 2005).

(iv) **LP93-21** was studied in detail by Kawka, Vennes & Ferrario (2020). It is suggested to be an ancient WD merger remnant with a mass of $1.1\,\mathrm{M_\odot}$. It is a warm carbon-dominated atmosphere DQ WD with a peculiar orbit in the Galaxy. Another team suggested that this WD is a type Iax supernova candidate (Ruffini & Casey 2019).

(v) **US-708** and Hyper-MUCHFUSS candidates (Hirsch et al. 2005; Tillich et al. 2011) identified one of the first HVSs and the first sdO HVS. Most of the Hyper-MUCHFUSS candidates identified by Ziegerer et al. (2017) do not not pass our quality thresholds. Specifically, the parallax measurements uncertainties are US-708: 0.067 ± 0.204 mas; SDSS J205030.39-061957.8: 0.17 ± 0.148 mas. SDSS J121150.27+143716: 0.0454 ± 0.1124 mas. SDSS J123137.56+074621.7 is not included, its parallax 0.2278 ± 0.0954. SDSS J163213.05+205124.0: 0.2629 ± 0.0961 mas. Finally, SDSS J164419.45+452326.7 is not included because its 2D velocity as derived from the proper motion is about $310\,\mathrm{km\,s^{-1}}$, which is far below our cut for the 2D velocity.

3 ANALYSIS

3.1 Objects selection: WDs with the largest proper motions in *Gaia* DR3

We search for hyper-runaway stars in *Gaia* data release 3 (Gaia Collaboration 2016, 2022). To do so, we first identify the fastest 1000 objects in the *Gaia* data base with colours and magnitudes compatible to WDs using similar magnitude and data quality cuts as Gentile Fusillo et al. (2021). We should note, however, that although most of the identified objects are consistent with being WDs, some were identified in various other studies to be hot subdwarfs stars of type B/O; these are listed in Table 1 as sdB/sdO, along with the relevant reference.

In order to perform our search we calculate the nominal 2D velocity taking:

$$v'\,[\mathrm{km\,s^{-1}}] = \frac{4.74\ \mu'\,[\mathrm{mas\,yr^{-1}}]}{\varpi'\,[\mathrm{mas}]}, \quad (1)$$

where μ' is the measured proper motion and ϖ' is the measured parallax. In order to exclude objects with large uncertainties, we included in our selection only objects which satisfy the following conditions: (1) $\varpi'/\sigma_{\varpi} > 4$, i.e. having a relative error of parallax measurement below 0.25; and (2) $\varpi' > 0.25$ mas, i.e. objects with nominal distances that are smaller than 4 kpc. We check the quality of the astrometric solution following the criteria of Fabricius et al. (2021), selecting only objects with (1) renormalized unit weight error (RUWE) < 1.4, (2) `IPD_FRAC_MULTI_PEAK` < 2, (3)

Table 1. The properties of HVS WDs. The units for the velocities are km s^{-1}; v_r is the radial velocity, v_t is transversal velocity, and $v_{\rm corr}$ is the transversal velocity corrected for rotation of the Milky Way and for *Gaia* parallax zero offset. In this correction, we assume that $R_\odot = 8.34$ kpc, $v_{\rm circ} = 240$ km s^{-1}, and the components of the peculiar solar velocity are $U = 11.1$ km s^{-1}, $V = 12.24$ km s^{-1}, and $W = 7.25$ km s^{-1}, which corresponds to works by Reid et al. (2014) and Schönrich, Binney & Dehnen (2010). Values in the last column corresponds to 95 per cent credible interval for the transversal velocity without correcting for the Milky Way rotation. The priors for velocity and distances are specified in Appendix B. The stellar types references are: (1) Kepler et al. (2015), (2) O'Donoghue et al. (2013), (3) Eisenstein et al. (2006), (4) Geier et al. (2017), (5) Green, Schmidt & Liebert (1986), (6) Kepler, Koester & Ourique (2016), (7) Brown et al. (2013), (8) Lamontagne et al. (2000) and (9) Smith et al. (2018).

Name	*Gaia* DR3 name	$\varpi' \pm \sigma_\varpi$ (mas)	$\mu \pm \sigma_\mu$ (mas yr^{-1})	Type	v_r (km s^{-1})	v_t (km s^{-1})	$v_{\rm corr}$ (km s^{-1})	Cred. interv. (km s^{-1})
HVUn 1	5703888058542880896	1.362 ± 0.318	207.876 ± 0.424	–	–	723.6	728.5	(574, 1770)
SDSS J125834.93-005946.1	3688712561723372672	1.419 ± 0.196	211.642 ± 0.334	DA(1)	140.62	706.8	693.5	(578, 1030)
HVsdBC 1	6368583523760274176	0.308 ± 0.065	36.638 ± 0.098	–	–	564.1	482.0	(402, 822)
HVWDC 1	6416314659255288704	1.894 ± 0.385	221.716 ± 0.492	–	–	555.0	527.4	(448, 1308)
HVWDC 2	6841322701358236416	2.787 ± 0.432	321.477 ± 0.475	–	–	546.7	531.9	(452, 938)
HVWDC 3	5808675437975384320	2.056 ± 0.368	232.483 ± 0.415	–	–	536.0	508.6	(442, 1156)
LSPM J1731+0331	4376935406816933120	2.056 ± 0.106	231.209 ± 0.126	–	–	533.0	525.3	(488, 600)
HVWDC 4	4739233769591077376	1.474 ± 0.214	165.588 ± 0.344	–	–	532.6	524.8	(434, 814)
HVUn 2	6640949596389193856	1.741 ± 0.158	193.175 ± 0.156	–	–	525.8	501.2	(458, 668)
HVWDC 5	4753345692095875328	6.489 ± 0.265	714.484 ± 0.354	–	–	521.9	518.0	(486, 570)
HVWDC 6	6777159394645734400	1.641 ± 0.322	169.82 ± 0.428	–	–	490.6	474.2	(392, 1040)
HVWDC 7	855361055035055104	17.332 ± 0.093	1782.657 ± 0.108	–	–	487.5	471.9	(482, 492)
EC 20559-3552	6778670265357654656	0.384 ± 0.067	37.951 ± 0.084	sdB (2)	–	469.0	445.8	(354, 672)
HVWDC 8	4943575978388814976	3.85 ± 0.624	380.566 ± 0.78	–	–	468.5	474.3	(384, 844)
HVWDC 9	2463291012727113216	3.542 ± 0.389	348.218 ± 0.528	–	–	465.9	449.3	(398, 636)
HVWDC 10	1241636356209099264	3.871 ± 0.333	379.02 ± 0.439	–	–	464.2	460.5	(406, 580)
HVWDC 11	5995439960564759296	2.842 ± 0.514	274.698 ± 0.688	–	–	458.1	437.1	(382, 1110)
LSPM J2224+1604	2737084320170352256	1.754 ± 0.28	167.723 ± 0.43	–	–	453.2	447.2	(372, 788)
HVWDC 12	2119975000945142272	1.551 ± 0.288	148.249 ± 0.591	–	–	453.1	446.4	(370, 980)
SDSS J123728.64+491302.6	1544331701176666624	1.042 ± 0.168	99.5 ± 0.19	DA (3)	−36.0	452.5	444.7	(358, 692)
LSPM J1345+3431	1470682632777169664	1.561 ± 0.276	148.647 ± 0.276	–	–	451.4	440.6	(358, 782)
SDSS J124743.35-134351.2	3528713077053554432	0.37 ± 0.09	34.637 ± 0.123	–	–	443.3	399.4	(298, 634)
HVWDC 13	729192473703851264	2.059 ± 0.432	191.878 ± 0.577	–	–	441.8	421.1	(348, 970)
FAUST 4434	6438915331219654400	0.868 ± 0.036	80.888 ± 0.041	sdOBHe (4)	–	441.7	415.6	(410, 482)
HVWDC 14	3537042874067950336	1.334 ± 0.101	123.765 ± 0.143	–	–	439.6	411.9	(388, 530)
HVWDC 15	1415765359864865408	5.146 ± 0.406	475.629 ± 0.751	–	–	438.1	436.3	(388, 536)
PG 1303+122	3737057611255721472	0.395 ± 0.059	35.903 ± 0.103	sdB (5)	−81.0	430.9	394.2	(326, 544)
HVsdBC 2	3195038476578336256	0.325 ± 0.078	29.504 ± 0.092	–	–	430.0	430.8	(282, 574)
HVWDC 16	4615529846653846016	3.48 ± 0.383	311.918 ± 0.749	–	–	424.8	401.1	(364, 586)
HVsdBC 3	6670029411202563584	0.322 ± 0.07	28.597 ± 0.097	–	–	420.5	410.1	(302, 660)
HVWDC 17	4925179671389315968	1.668 ± 0.318	147.564 ± 0.413	–	–	419.3	402.8	(332, 804)
HVWDC 18	2914272062095015552	1.98 ± 0.336	174.78 ± 0.444	–	–	418.3	416.6	(342, 798)
LSPM J1240+6710	1682129610835350400	2.36 ± 0.119	208.248 ± 0.193	DS (6)	–	418.3	412.2	(382, 468)
SDSS J123800.09+194631.4	3948319763985443200	0.452 ± 0.099	39.747 ± 0.14	D (7)	−69.0	416.5	397.3	(286, 568)
Ton S 145	2335322500798589184	0.419 ± 0.082	36.657 ± 0.094	sdBHe1 (8)	–	415.1	404.9	(292, 548)
HVUn 3	2654214506741818880	3.397 ± 0.631	297.383 ± 1.041	–	–	414.9	402.8	(338, 920)
HVWDC 19	3611573712136684928	2.067 ± 0.44	180.325 ± 0.615	–	–	413.5	391.0	(330, 1002)
HVUn 4	4026695083122023552	4.122 ± 0.816	358.18 ± 1.118	–	–	411.8	406.3	(334, 986)
HVWDC 20	6414789778364569216	2.069 ± 0.226	178.333 ± 0.307	–	–	408.5	381.6	(350, 562)
PG 1608+374	1378348017099023360	0.268 ± 0.049	23.111 ± 0.08	sdOHe (1)	–	408.3	383.2	(290, 514)
HVWDC 21	2497775064628920832	3.719 ± 0.302	318.334 ± 0.426	–	–	405.7	391.3	(358, 500)
HVWDC 22	5142197118950177280	13.036 ± 0.097	1111.31 ± 0.109	–	–	404.1	400.5	(398, 410)
HVWDC 23	1217609832414369536	7.336 ± 0.759	624.631 ± 1.191	–	–	403.6	397.2	(348, 544)
2MASS J12564352-6202041	5863122429179888000	13.237 ± 0.326	1124.303 ± 0.421	L (9)	–	402.6	385.2	(384, 424)
HVWDC 24	3905910019954089856	3.291 ± 0.332	279.459 ± 0.478	–	–	402.5	404.4	(346, 530)
HVWDC 25	1212348119518459392	11.217 ± 0.353	951.562 ± 0.54	–	–	402.1	399.8	(380, 430)

`IPD_GOF_HARMONIC_AMPLITUDE` < 0.1, and (4) `ASTROMETRIC_SIGMA5D_MAX` < 1.5. We then apply the colour-magnitude cut suggested by Gentile Fusillo et al. (2021):

$$G_{\rm abs} > 6 + 5(G_{\rm BP} - G_{\rm RP}). \quad (2)$$

Our complete ADQL request can be found in Appendix A. We summarize the essential information about candidates with $v' >$ 400 km s^{-1} in Table 1. We search for the names and properties of these objects in the Simbad data base (Wenger et al. 2000).

In this search we identified for the first time 32 new hyper-runaway WD and sdB candidates. We give these candidates composite names with an 'HV' prefix (standing for high-velocity) followed by the object type and their sequential number. We summarize the number of new found candidates in Table 2. We explain how we assign the candidate types later on.

Table 2. Number of newly found hyper-runaway stars.

Identificator	Type of hyper-runaway stars	Number
Newly identified WDs and sdBs		32
HVWDC	... of which WDs	25
HVsdBC	... of which sdBs	3
HVUn	... of which unknown nature	4
HVsMSC	Newly identified sub-MS	14
	... of which unbound (hypervelocity)	2

It is known that quasars in *Gaia* EDR3 have an average parallax of $-17\,\mu$as (Lindegren et al. 2021). This value varies with the magnitude and the location of the star and is summarized in the `Python` package `gaiadr3-zeropoint`.[3] It was shown in previous works (Marchetti, Rossi & Brown 2019; Marchetti 2021) that accounting for the zero-point offset has a significant impact on the number of stars which appear to be unbound to the Galaxy. The effect is relatively small in our work because we limit the minimal parallax to 0.250 mas. We can estimate the maximum amplitude of the change as $(17/250) \times 450 \approx 30\,\mathrm{km\,s^{-1}}$. We compute velocities corrected for the motion of the LSR and zero point in Table 1 as $v_{\rm corr}$. The maximum change due to the zero-point offset is around $10\,\mathrm{km\,s^{-1}}$.

The parallax is measured with significantly worse precision in comparison to the proper motion for the majority of these candidates. Therefore, parallax uncertainty contributes significantly to the uncertainty of the 2D velocity. The parallax measurement is subject to the Lutz–Kelker bias (Lutz & Kelker 1973). Two factors contribute to this bias: (1) a symmetric normal distribution for the parallax errors translates into a right-skewed error distribution for the distances, and (2) there are more stars at larger distances from the Sun in comparison to smaller distances, thus in any parallax-limited sample, the distances are more likely to be underestimated. Since the 2D velocity is proportional to the distance, the nominal velocities in our parallax-limited sample are also expected to be underestimated. Fortunately, there are known mitigation techniques to deal with the Lutz–Kelker bias (Bailer-Jones 2015; Igoshev, Verbunt & Cator 2016). We write the Bayesian posterior for the 2D velocities. The posterior estimate for the velocity is a multiplication of the conditional probabilities to measure a parallax given a distance, the conditional probabilities to measure components of proper motion given a velocity and priors for the velocity and the distance. For the distance, we use the Galactic prior suggested by Verbiest et al. (2012). For the velocity, we use a prior composed of two multiplied normal distributions with $\sigma = 1000\,\mathrm{km\,s^{-1}}$. The details of this calculation are summarized in Appendix B. We estimate the 95 per cent credible interval for each object and provide them in the last column of Table 1. We make our code calculating posterior velocities publicly available.[4]

3.2 Distribution of HVS candidates in the Hertzsprung–Russell diagram

We plot the locations of the HVS candidates on the Hertzsprung–Russell diagram in Fig. 1. There are three different classes of sources present at this diagram: (1) WD-like sources coincide or are slightly above the WD sequence, (2) hot subdwarf B-like sources

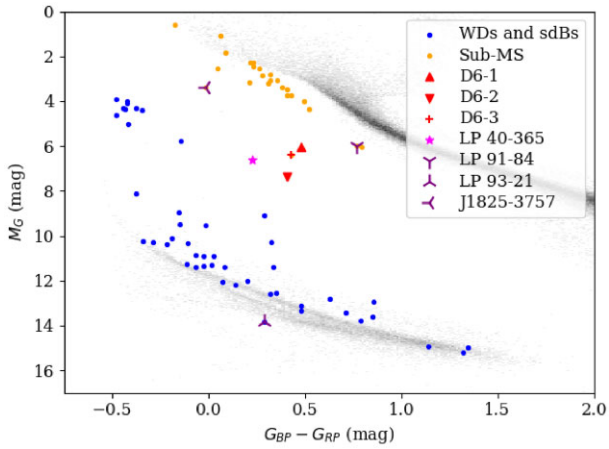

Figure 1. Hertzsprung–Russell diagram for WDs, sdBs, and sub-MS candidates with the largest nominal 2D velocities. The *Gaia* 100 pc sample is plotted in grey-scale for reference.

are concentrated around $G \approx 4$ and $G_{\rm Bp} - G_{\rm Rp} \approx -0.4$, and (3) sources located between the WD sequence and the main sequence (MS), including DR6-1, DR6-2, and DR6-3 earlier identified by Shen et al. (2018).

Some hot subdwarf O and B stars are known as HVS sources (see Heber 2009, for a review and references). For example, the sdO star US 708 (not included in our sample because $\varpi' = 0.0672 < 0.25$ mas) has a radial velocity of $708 \pm 15\,\mathrm{km\,s^{-1}}$ (Hirsch et al. 2005). Moreover, up to 20 per cent of sdB stars belong to the Milky Way halo (Napiwotzki 2008), thus their velocities are expected to be hundreds of $\mathrm{km\,s^{-1}}$ with respect to the LSR of the thin disc. We classify candidates with $4 \leq M_G \leq 6$ and $-0.5 \leq G_{\rm BP} - G_{\rm RP} \leq -0.25$ as HVsdBC, i.e. high-velocity sdB candidates.

3.3 Additional data for the HVS WD candidates

Some additional data exist for other candidates that were not previously identified as HVS. These objects might be of special interest due to their velocities.

In Table 3, we present the estimates of the mass and temperature of our candidate WDs taken from Gentile Fusillo et al. (2021). In the following we briefly summarize our knowledge about these and other candidates from the Gentile Fusillo et al. study and other sources. Gentile Fusillo et al. (2021) assigns each WD candidate a parameter, $P_{\rm WD}$, indicating its probability of being a WD. We classify stars high $P_{\rm WD}$ and fitted WD model atmosphere as HVWDC i.e. HVS WD candidates. It leaves us with four stars, *Gaia* DR3 5703888058542880896, 6640949596389193856, 2654214506741818880, and 4026695083122023552, which have a small probability of being WDs ($P_{\rm WD} < 0.9$), while their magnitudes and colours seem to be incompatible with sdBs. We classify these as HVUn i.e. high-velocity unknown nature. These objects, that require additional spectral investigation, are among the most interesting sources found in this work.

(i) LSPM J1240+6710/*Gaia* DR3 1682129610835350400 (Kepler et al. 2016) studied this WD due to its unique atmospheric composition, significantly dominated by oxygen. They proposed it is related to an atypical stellar evolution, likely involving a violent very-late thermal pulse during the post-asymptotic giant branch (AGB) stage. However, such evolution should not provide any velocity kick. Gänsicke et al. (2020) found that this object has high

[3] https://pypi.org/project/gaiadr3-zeropoint/
[4] https://pypi.org/project/post-velocity/

Table 3. Physical properties of hyper-runaway WDs found by Gentile Fusillo et al. (2021). Here P_{wd} is the probability of object to be a WD, $T_{eff,H}$, H, and M_H correspond to temperature and mass estimated if the compositions is pure hydrogen. $T_{eff\,He}$ and M_{He} correspond to pure helium composition. We also provide two χ^2 values by Gentile Fusillo et al. (2021) for hydrogen and helium atmosphere compositions as χ^2(H), χ^2(He), respectively.

SDSS	*Gaia* DR3	P_{wd}	$T_{eff,H}$	M_H	χ^2(H)	$T_{eff,He}$	M_{He}	χ^2(He)
	5703888058542880896	0.447						
J125834.93-005946.1	3688712561723372672	0.963	11453.8 ± 1445.1	0.146 ± 0.051	0.04	12251.4 ± 1525.0	0.176 ± 0.073	0.76
	6368583523760274176	0.011						
	6416314659255288704	0.727	8880.7 ± 1232.1	0.268 ± 0.169	0.01	8866.3 ± 1362.5	0.266 ± 0.161	0.05
	6841322701358236416	0.994	12669.3 ± 2004.7	0.462 ± 0.157	2.91	12666.3 ± 1762.8	0.463 ± 0.173	5.21
	5808675437975384320	0.996	14560.4 ± 3163.4	0.524 ± 0.242	1.41	14511.5 ± 3087.8	0.512 ± 0.276	2.85
	4376935406816933120	0.99	24160.0 ± 1473.1	0.391 ± 0.033	32.58	27730.5 ± 2018.4	0.41 ± 0.021	24.42
	4739233769591077376	0.999	25986.7 ± 6911.6	0.603 ± 0.278	0.02	30549.4 ± 10543.3	0.68 ± 0.285	0.1
	6640949596389193856	0.237						
	4753345692095875328	0.944	5626.9 ± 352.9	0.357 ± 0.098	0.79	5575.2 ± 326.2	0.354 ± 0.094	0.87
	6777159394645734400	0.998	22445.8 ± 5002.5	0.488 ± 0.208	0.61	26274.1 ± 7204.0	0.527 ± 0.203	1.16
J104559.14+590448.2	855361055035055104	1.0	8720.9 ± 183.1	1.049 ± 0.025	0.29	8505.6 ± 168.4	1.0 ± 0.026	0.76
	6778670265357654656	0.008						
	4943575978388814976	0.976	7076.2 ± 1410.6	0.57 ± 0.412	0.16	6952.2 ± 1403.7	0.515 ± 0.414	0.17
J015938.43-081242.3	2463291012727113216	0.966	8305.5 ± 1127.6	0.469 ± 0.247	2.1	8216.6 ± 1135.2	0.47 ± 0.227	1.96
J144205.71+220328.1	1241636356209099264	0.979	8638.9 ± 938.5	0.535 ± 0.203	0.02	8464.9 ± 910.6	0.473 ± 0.174	0.05
	5995439960564759296	0.985	15469.5 ± 4435.2	0.807 ± 0.333	0.61	14078.3 ± 3745.7	0.725 ± 0.354	0.17
J222403.94+160405.0	2737084320170352256	0.997	17197.0 ± 4372.3	0.376 ± 0.148	7.91	18740.0 ± 5577.2	0.431 ± 0.2	10.11
	2119975000945142272	0.978	12084.9 ± 3110.8	0.37 ± 0.165	0.38	12363.5 ± 2868.2	0.38 ± 0.222	0.89
J123728.64+491302.6	1544331701176666624	0.969	13948.4 ± 1630.4	0.152 ± 0.061	0.87	14465.3 ± 1445.0	0.181 ± 0.068	3.41
J134503.42+343140.6	1470682632777169664	0.996	14517.6 ± 2597.4	0.349 ± 0.112	0.18	14340.6 ± 2320.8	0.361 ± 0.119	0.05
J124743.35-134351.2	3528713077053554432	0.047						
J103239.96+282724.9	729192473703851264	0.996	13354.5 ± 3582.8	0.527 ± 0.288	1.96	13121.5 ± 3310.7	0.486 ± 0.333	3.07
	6438915331219654400	0.012						
	3537042874067950336	0.932	35775.4 ± 4798.4	0.375 ± 0.061	4.94			
	1415765359864865408	0.969	6112.5 ± 649.1	0.494 ± 0.219	4.4	6008.1 ± 639.5	0.48 ± 0.206	4.31
J130543.96+115840.8	3737057611255721472	0.007						
	3195038476578336256	0.012						
	4615529846653846016	0.853	6919.0 ± 756.9	0.351 ± 0.159	0.7	6805.0 ± 740.6	0.343 ± 0.139	0.66
	6670029411202563584	0.014						
	4925179671389315968	0.991	12476.4 ± 3096.7	0.388 ± 0.186	0.13	12644.2 ± 2953.6	0.397 ± 0.237	0.0
	2914272062095015552	0.982	10992.6 ± 1495.3	0.421 ± 0.184	0.65	10976.6 ± 1641.5	0.405 ± 0.171	1.43
	1682129610835350400	0.999	22494.9 ± 4178.4	0.514 ± 0.129	0.13	25261.6 ± 7590.0	0.536 ± 0.072	0.0
J123800.09+194631.4	3948319763985443200	0.188						
	2335322500798589184	0.028						
J223808.19+003247.6	2654214506741818880	0.624						
	3611573712136684928	0.998	14549.2 ± 4194.3	0.514 ± 0.307	1.83	14440.2 ± 4068.7	0.498 ± 0.359	3.04
J120037.57+320330.7	4026695083122023552	0.887						
	6414789778364569216	0.998	17801.3 ± 3379.0	0.464 ± 0.149	0.0	17422.9 ± 4240.0	0.464 ± 0.213	0.28
J161023.39+371315.9	1378348017099023360	0.011						
J024837.53-003123.9	2497775064628920832	0.973	9860.0 ± 1338.0	0.489 ± 0.211	6.77	9510.6 ± 1358.8	0.451 ± 0.168	7.86
J014809.10-171222.0	5142197118950177280	0.987	7268.0 ± 130.0	0.515 ± 0.033	6.44	7138.0 ± 127.0	0.461 ± 0.011	6.11
J153719.45+223727.6	1217609832414369536	0.969	4553.5 ± 568.9	0.415 ± 0.309	0.88	4626.6 ± 434.6	0.442 ± 0.272	0.89
	5863122429179888000	0.995	4561.6 ± 181.8	0.521 ± 0.093	4.88	4587.7 ± 145.0	0.512 ± 0.08	4.98
J120722.82+091722.3	3905910019954089856	0.993	10812.7 ± 1731.5	0.628 ± 0.251	0.28	10846.8 ± 1947.1	0.564 ± 0.242	0.08
J151530.71+191130.8	1212348119518459392	0.958	4424.0 ± 363.3	0.401 ± 0.152	0.2	4533.9 ± 271.0	0.435 ± 0.135	0.2

velocity of ≈250 km s^{-1} in the direction opposite to the Milky Way rotation.

Instead, here we suggest that our identification of this WD as a HVS WD, together with its unique composition, that includes even traces of Si, could be consistent with the scenario for Iax SN suggested by one of us (Jordan et al. 2012). There we proposed that a near-Chandrasekhar WD experiences an explosive asymmetric partial deflagration event which burns only a fraction of the WD, but leaves behind a bound partially burnt WD remnant, which is ejected at a high velocity (due to the asymmetric explosion). The atmosphere of such a WD would also be polluted by fall-back burnt material, potentially consistent with the observations of SDSS J123800.09+194631.4.

(ii) SDSS J015938.43-081242.4 is a WD of type DA (Kilic et al. 2006).

(iii) EC 20559-3552 is classified as a hot subdwarf (O'Donoghue et al. 2013) with a $U - B$ colour of −1.1.

We show mass distribution of candidates with derived mass by Gentile Fusillo et al. (2019) in Fig. 2. Our HVS candidates seems to be slightly less massive than local WDs. It might be a result of observational bias, because low-mass WDs have larger radii and thus are expected to be brighter than high-mass WDs. Since our sample is parallax limited, we naturally tend to discover more bright sources.

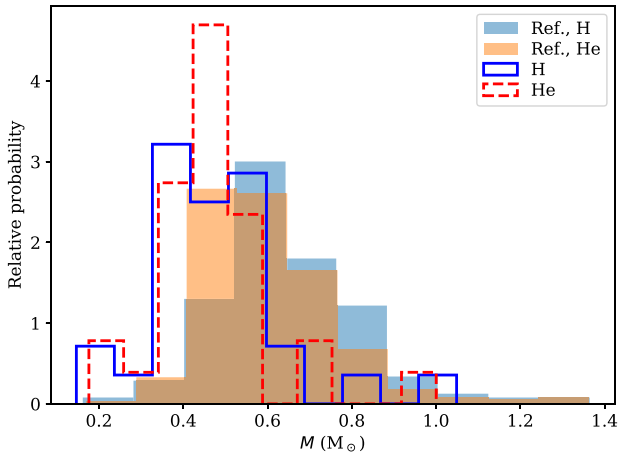

Figure 2. Distribution of derived masses for HVS WD candidates (solid and dashed lines) in comparison to local WD population with $\varpi' > 20$ (filled histograms). Mass measurements are taken from catalogue by Gentile Fusillo et al. (2021).

3.4 Sub-main-sequence peculiar candidates

Our strict filtering procedure described in the previous section did not identify some known hyper-runaway objects suspected to be related to WDs ejected following a thermonuclear SN explosion (e.g. the D6-1, D6-2, and D6-3 objects found by Shen et al. 2018). In order to identify these candidates and allow for the possible identification of peculiar objects, which might not resemble normal WDs, we select an additional sample of hyper-runaway candidates for which we relax our magnitude selection criteria replacing it with the following:

$$G_{\rm abs} > 6.67(B_p - R_p) + 0.66. \quad (3)$$

In this case, we select for objects which are positioned just below the MS. Our ADQL request for these candidates can also be found in Appendix A. This gives rise to the identification of not only sub-MS objects, but also potential MS hyper-runaway stars. Such MS stars are selected although they appear to reside below the MS because their measured parallax is overestimated in comparison to real parallax, thus their absolute magnitude is underestimated. While also of interest, the latter MS candidates are not the focus of our current paper. In order to limit the number of these objects, we additionally impose a cut of $v' > 550\,{\rm km\,s^{-1}}$ to this sample. Our final sub-MS candidates are shown in Table 4. Newly discovered sources were given a designation HVsMSC, i.e. hyper-runaway sub-MS candidates.

4 OBJECTS OF SPECIAL INTEREST AND PRIME TARGETS FOR FOLLOW-UP CHARACTERIZATION

Here, we first discuss our new prime candidates for follow-up observations, and then briefly discuss candidates in our WD and sub-MS samples, and any studies already done on any of these candidates.

4.1 HVS WD candidates

We find four new sources which have velocities exceeding $700\,{\rm km\,s^{-1}}$ and are likely (with the caveat of large measurement uncertainties) unbound from the Galaxy, and therefore require a significant velocity kick. Two of these are found in our WD sample, HVUn 1 (*Gaia* DR3 5703888058542880896) and SDSS J125834.93-005946.1/*Gaia* DR3 3688712561723372672, where SDSS J125834.93-005946.1 also has a known radial-velocity measurement of $140\,{\rm km\,s^{-1}}$. Another two likely unbound HVS sources were found in our second sample of sub-MS HVS candidates: SDSS J145847.01+070754.4 and BPS BS 16470-0087.

Given their kinematics, all four sources are prime targets for follow-up observations to better characterize their properties.

4.2 Bound/marginally bound hyper-runaway WDs

Monari et al. (2018) find the local escape velocity from the Galaxy to be $580 \pm 63\,{\rm km\,s^{-1}}$, and suggest it decreases monotonically between $640\,{\rm km\,s^{-1}}$ at 4 kpc to $550\,{\rm km\,s^{-1}}$ at 11 kpc (Galactocentric distances). It is therefore likely that our two fastest new HVS WD candidates are unbound HVS WDs kicked following an explosive event, or strong dynamical interaction. The next 8 candidates in Table 1 have tangential velocities ranging between 520–565 $\rm km\,s^{-1}$. A non-negligible radial-velocity component could potentially make these WDs be unbound HVS WDs, but overall these might bound WDs, in which case they are likely to be on highly eccentric orbits. In principle, these just might be the extreme tail of normal halo WDs. Distinguishing between these possibilities requires knowledge on the radial-velocity component and/or a good age estimate, given that halo WDs are expected to be old. We have searched for archival data of radial velocities for these objects but found no additional data.

Since halo-formed WDs originate from very old (>10 Gyr; Jofré & Weiss 2011; Kilic et al. 2019) populations, identifying younger WDs among these would suggest a disc origin, and hence a large kick, in order to explain their measured velocities. WDs involved in a SN explosion might also have been heated through accretion of material (dynamical detonation in the double-degenerate case; Shen et al. 2018) or a weak deflagration (for the Iax SNe, as we originally suggested; Jordan et al. 2012), and appear peculiar and/or younger. D6-1–D6-3 for example, have peculiar positions on the HR diagram, suggested to be related to material accretion from the exploding companion (Shen et al. 2018), while LP 93-21 shows a peculiar composition, suggested to be related to a Iax SN (Ruffini & Casey 2019), and similarly (Vennes et al. 2017; Raddi et al. 2018b) for the LP 40-365 object.

For a sub-sample of our candidates, we can estimate the WD cooling ages, as well as the total ages (since zero-age MS), using the `WD_models` PYTHON package.[5] However, this approach is limited to more massive WDs. WDs of masses lower than $0.5\,{\rm M_\odot}$ could not form through normal stellar evolution of single stellar progenitor over a Hubble time. These He or hybrid HeCO WDs (Zenati, Toonen & Perets 2019) have likely undergone a binary evolution stripping process. It is therefore, difficult to estimate their true age, in that case, we cannot exclude a halo origin. To some extent, this could also be the case for slightly more massive WDs, which might have been affected by binary evolution, even if their mass is consistent with the age of the Galaxy, in which case, their total ages might appear older than they are. The WDs with estimated masses and ages are shown in Table 5. We plot constant age contours for WDs in Fig. 3. We also compute the kinematic ages as b/μ_b for WDs where the sign of proper motion in latitudinal direction coincides with the sign of Galactic latitude. Typical oscillations in the Galactic gravitational potential occur on time-scales comparable to 100 Myr, thus even WDs with cooling ages of 0.2–0.5 Gyr could have completed a few

[5] https://github.com/SihaoCheng/WD_models

Table 4. The properties of hyper-runaway objects. The units for velocities are km s^{-1}; v_r is the radial velocity, v_t is transversal velocity and $v_{\rm corr}$ is the transversal velocity corrected for rotation of the Milky Way and for *Gaia* parallax zero offset. In this correction, we assume that $R_\odot = 8.34$ kpc, $v_{\rm circ} = 240$ km s^{-1}, and the components of the peculiar solar velocity are $U = 11.1$ km s^{-1}, $V = 12.24$ km s^{-1}, and $W = 7.25$ km s^{-1}, which correspond to works by Reid et al. (2014) and Schönrich et al. (2010). Values in the last column correspond to 95 per cent credible interval for transversal velocity without correcting for the Milky Way rotation. Priors for the velocity and distances are specified in Appendix B. The stellar types references are: (1) Brown et al. (2008), (2) Sayres et al. (2012), (3) Lynn et al. (2004), and (4) Greenstein (1969). The radial velocities of D6-1, D6-2, and D6-3 candidates are from Shen et al. (2018).

Name	*Gaia* DR3 name	$\varpi' \pm \sigma_\varpi$ (mas)	$\mu \pm \sigma_\mu$ (mas yr^{-1})	Type	v_r (km s^{-1})	v_t (km s^{-1})	$v_{\rm corr}$ (km s^{-1})	Cred. interv. (km s^{-1})
LSPM J1852+6202/D6-3	2156908318076164224	0.423 ± 0.099	211.996 ± 0.202	–	20	2374.3	2313.6	(1552, 2470)
D6-1	5805243926609660032	0.531 ± 0.07	211.749 ± 0.088	–	1200	1890.5	1736.8	(1512, 2370)
LP 398-9/D6-2	1798008584396457088	1.194 ± 0.065	259.514 ± 0.089	–	20	1030.6	1024.4	(938, 1166)
SDSS J145847.01+070754.4	1160986392332702720	0.407 ± 0.032	62.771 ± 0.044	–	− 117.0	730.6	656.8	(630, 852)
BPS BS 16470-0087	3946876384391994496	0.4 ± 0.023	59.154 ± 0.031	A1.7 (1)	76.0	700.4	620.9	(624, 778)
HVsMSC 1	3734729567182624512	0.333 ± 0.045	48.26 ± 0.075	–	–	687.0	606.1	(526, 828)
J1825-3757	6727110900983876096	1.051 ± 0.028	147.814 ± 0.033	–	− 47.0	666.5	627.0	(634, 704)
HVsMSC 2	2316981409896303232	0.564 ± 0.035	75.776 ± 0.047	–	–	636.8	584.1	(566, 720)
LP 91-84	1063044954547608064	1.665 ± 0.022	219.672 ± 0.026	sdB (2)	–	625.6	601.1	(610, 642)
HVsMSC 3	5814962273679342208	0.402 ± 0.023	52.708 ± 0.024	–	–	621.8	525.8	(564, 708)
HVsMSC 4	3792840680855962240	0.46 ± 0.035	60.13 ± 0.051	–	–	619.9	541.6	(538, 718)
PHL 5459	6610315175214347264	0.407 ± 0.023	52.446 ± 0.029	–	–	610.4	537.5	(548, 678)
HVsMSC 5	1244274913532995072	0.26 ± 0.061	33.307 ± 0.068	–	–	608.0	533.6	(380, 700)
HVsMSC 6	5114953763436002816	0.369 ± 0.027	47.071 ± 0.039	–	–	604.6	529.4	(524, 694)
HVsMSC 7	6683685723576804992	0.29 ± 0.022	36.799 ± 0.025	–	261.0	600.7	517.0	(524, 702)
HVsMSC 8	4426088459959127552	0.274 ± 0.028	34.592 ± 0.037	–	–	599.2	510.4	(494, 718)
HVsMSC 9	1480060406106959232	0.307 ± 0.019	38.322 ± 0.025	–	–	592.5	528.3	(520, 660)
SDSS J145110.86+335624.2	1292695756353196800	0.26 ± 0.036	32.365 ± 0.045	–	–	590.6	534.7	(442, 692)
HVsMSC 10	2328667912829146368	0.385 ± 0.047	47.513 ± 0.056	–	–	585.7	511.7	(464, 718)
EC 00179-6503	4900121354714539136	0.453 ± 0.016	55.444 ± 0.024	sdO (3)	71.0	579.8	504.9	(542, 622)
HVsMSC 11	6849636078710196608	0.335 ± 0.024	40.165 ± 0.029	–	–	568.6	484.2	(500, 660)
SDSS J171531.67+271545.5	4574342862635194368	0.403 ± 0.025	48.077 ± 0.035	–	− 245.5	565.9	529.2	(506, 646)
GD 159	1244919124267663488	0.94 ± 0.019	111.472 ± 0.023	A (4)	–	561.8	528.0	(540, 584)
HVsMSC 12	3924826739553387648	0.468 ± 0.051	55.205 ± 0.065	–	–	559.5	497.7	(456, 684)
HVsMSC 13	4937802236674281088	0.455 ± 0.072	53.262 ± 0.112	–	–	554.5	519.0	(418, 734)
HVsMSC 14	4992603393106801920	0.281 ± 0.042	32.739 ± 0.06	–	–	553.0	479.0	(406, 652)

Table 5. The estimated masses, cooling ages, and total ages of WD HVS candidates located on the WD cooling sequence, assuming these are Solar metallicity CO-core DA WDs. The WD parameters were estimated using the models of Bédard et al. (2020), while the progenitor lifetimes were estimated using the models of Choi et al. (2016). b is the Galactic latitude, μ_b is proper motion in the direction of Galactic latitude, and $t_{\rm kin}$ is the kinematic age computed as minimal time required to reach the galactic latitude b.

Name	*Gaia* DR3 name	$M_{\rm WD}$ ($M_\odot$)	Cooling age (Gyr)	Total age (Gyr)	b (°)	μ_b (mas yr^{-1})	$t_{\rm kin}$ (Gyr)
HVWDC 4	4739233769591077376	0.54	0.0223	5.29	− 55.997	164.491	
HVWDC 7	855361055035055104	1	3.17	3.26	51.415	221.851	0.0008
HVWDC 8	4943575978388814976	0.61	1.52	3.15	− 65.471	184.841	
HVWDC 11	5995439960564759296	0.59	0.631	2.81	8.647	− 25.583	
HVWDC 24	3905910019954089856	0.64	0.576	1.84	69.348	− 169.926	
HVWDC 10	1241636356209099264	0.51	0.835	13.4	64.394	− 134.903	
HVWDC 13	729192473703851264	0.52	0.264	10.3	59.386	− 166.109	
HVWDC 19	3611573712136684928	0.52	0.203	9.44	50.884	12.157	0.0151
HVWDC 22	5142197118950177280	0.5	1.19	14.3	− 73.568	− 787.062	0.0003
HVWDC 23	1217609832414369536	0.55	6.03	9.83	52.274	− 30.262	

oscillations if they are bound. The only source with comparable kinematic and cooling age is *Gaia* DR3 3611573712136684928, but even in this case the cooling age is only one order of magnitude larger than kinematic age.

Eventually, we are left with five candidates with estimated total ages significantly shorter than the halo stellar population; HVWDC 4, 7, 8, 11, and 24. These WDs are therefore prime targets for follow-up spectroscopic observations to constrain their 3D velocity, chemical compositions, and physical properties.

In order to potentially provide an alternative age estimates for the other candidates, we also provide the height of the observed WDs above the disc, see Fig. 4. Casagrande et al. (2016) show that the vast majority of stars residing below 1 kpc from the plane are stars younger than the 10 Gyr age of halo stars. Most of our HVS WD candidates reside below 1 kpc from the plane with the majority below 0.5 kpc (see Table 6). These findings are consistent with a disc origin for the majority of the sample. One should note that due to their low luminosities, one cannot identify very far WDs, which therefore

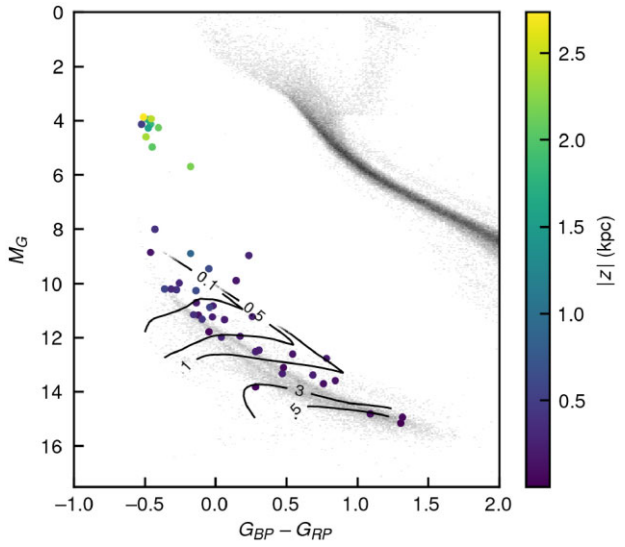

Figure 3. The HVS WD candidate de-reddened (using Capitanio et al. 2017) location on the *Gaia* HR diagram, coloured by the absolute height above/below the Galactic disc. Theoretical cooling-age isochrones for DA WDs (Bédard et al. 2020) are shown in black (the labels mark the cooling age in Gyr). The *Gaia* 100 pc sample is plotted in grey-scale for reference.

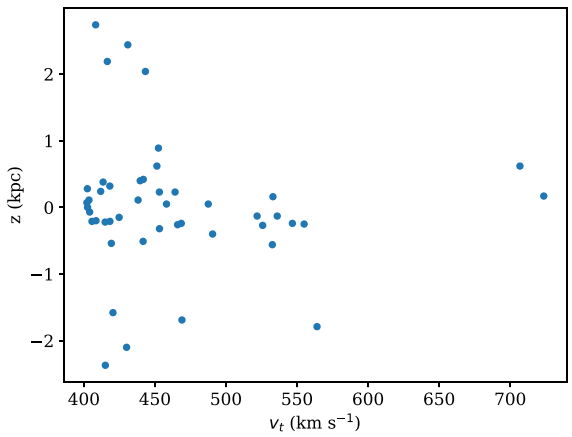

Figure 4. Distribution of transversal velocities and heights above the Galactic plane for hyper-runaway WD candidates.

a priori limits the largest distances, and hence also the heights above the disc.

We conclude that excluding a halo origin for any individual WD (with no age estimate) in our sample is challenging, but that most of our candidate HVS WDs are likely to have a disc origin, and require a non-trivial velocity kick. Nevertheless, radial-velocity follow-ups are required to better constrain/confirm their origin.

4.2.1 LSPM J1240+6710/Gaia DR3 1682129610835350400

For this WD, we could infer a high mass of ∼0.79 $M_\odot$ and a small cooling age of about 0.03 Gyr. In a detailed spectroscopic observations its mass was estimated as 0.41 $M_\odot$ (Gänsicke et al. 2020). Given that the progenitor mass of such WDs is 3–4 $M_\odot$ (with MS lifetimes of ∼400–500 Myr), such WD cannot be a halo WD, and therefore likely originated in the disc. Its ∼420 km s^{-1} tangential velocity (and measured 177 km s^{-1} radial velocity) therefore makes it a very high velocity runaway, requiring some evolution of dynamical velocity excitation mechanism. Furthermore, it is a oxygen dominated WD. Interestingly, this WD has been indeed already identified independently as a potential partly burnt SN remnant by Gänsicke et al. (2020), due to its peculiar atmospheric composition derived from follow-up observations. Our independent identification of this candidate by its velocity (and exclusion as a halo WD), rather than the previous identification due to its unique spectral features, further supports our approach in identifying potential WDs related to SN explosions.

Table 6. Apparent magnitudes, absolute magnitudes, colours, Galactocentric distances, and heights above the Galactic plane for hyper-runaway WD candidates. The Galactocentric distance is computed assuming $R_\odot = 8.5$ kpc.

Gaia DR3 name	g (mag)	G (mag)	Bp–Rp (mag)	R (kpc)	z (kpc)
5703888058542880896	19.6	10.27	0.32	8.81	0.17
3688712561723372672	18.77	9.53	−0.02	8.31	0.62
6368583523760274176	16.87	4.31	−0.37	6.78	−1.79
6416314659255288704	20.0	11.39	0.34	8.14	−0.25
6841322701358236416	19.1	11.32	0.02	8.29	−0.24
5808675437975384320	19.8	11.37	−0.03	8.14	−0.13
4376935406816933120	17.93	9.49	−0.15	8.09	0.16
4739233769591077376	19.41	10.25	−0.34	8.42	−0.56
6640949596389193856	17.88	9.09	0.29	8.02	−0.27
4753345692095875328	19.54	13.6	0.85	8.51	−0.13
6777159394645734400	19.29	10.37	−0.21	8.04	−0.4
855361055035055104	17.64	13.83	0.29	8.53	0.05
6778670265357654656	16.16	4.08	−0.42	6.54	−1.69
4943575978388814976	20.43	13.36	0.48	8.51	−0.24
2463291012727113216	19.81	12.55	0.35	8.62	−0.26
1241636356209099264	19.66	12.6	0.32	8.4	0.23
5995439960564759296	19.91	12.17	0.14	8.19	0.05
2737084320170352256	18.91	10.13	−0.19	8.42	−0.32
2119975000945142272	19.98	10.93	0.03	8.4	0.23
1544331701176666624	18.86	8.95	−0.15	8.73	0.89
1470682632777169664	19.37	10.33	−0.11	8.45	0.62
3528713077053554432	17.2	5.04	−0.42	7.72	2.04
729192473703851264	19.82	11.39	−0.07	8.73	0.42
6438915331219654400	14.61	4.3	−0.44	7.59	−0.51
3537042874067950336	17.49	8.12	−0.38	8.48	0.4
1415765359864865408	20.21	13.77	0.79	8.47	0.11
3737057611255721472	16.02	4.0	−0.42	8.03	2.44
3195038476578336256	16.83	4.39	−0.34	10.65	−2.1
4615529846653846016	20.09	12.79	0.63	8.39	−0.15
6670029411202563584	16.82	4.37	−0.43	5.9	−1.58
4925179671389315968	19.81	10.92	−0.03	8.34	−0.54
2914272062095015552	19.9	11.38	0.08	8.8	−0.21
1682129610835350400	18.4	10.27	−0.29	8.66	0.32
3948319763985443200	17.49	5.76	−0.14	8.45	2.19
2335322500798589184	16.52	4.63	−0.48	8.25	−2.37
2654214506741818880	20.27	12.92	0.86	8.43	−0.22
3611573712136684928	19.66	11.24	−0.11	8.27	0.38
4026695083122023552	20.36	13.44	0.71	8.55	0.24
6414789778364569216	19.28	10.86	−0.07	8.17	−0.2
1378348017099023360	16.79	3.93	−0.48	7.54	2.74
2497775064628920832	19.17	12.02	0.2	8.67	−0.21
5142197118950177280	17.54	13.11	0.48	8.52	−0.07
1217609832414369536	20.59	14.91	1.14	8.43	0.11
5863122429179888000	19.58	15.19	1.32	8.46	0.0
3905910019954089856	19.47	12.06	0.07	8.5	0.28
1212348119518459392	19.75	15.0	1.35	8.46	0.07

Table 7. Possible association between hyper-runaway WD and SNRs. d is the minimal angular distance between SNR centre and past trajectory of the star, and t is the time of the closest approach.

Gaia DR3 name	SNR name	SNR min angular size (arcmin)	d (arcmin)	t kyr
5863122429179888000	G308.8-00.1	20.0	− 6.12	36658.24
5863122429179888000	G309.8+00.0	19.0	14.46	43040.1
5863122429179888000	G310.8-00.4	12.0	5.52	50656.81
5863122429179888000	G315.4-02.3	42.0	6.37	85085.09

4.3 Peculiar hyper-runaway/HVS objects below the MS

4.3.1 DR6-1, DR6-2, DR6-3

These objects were the main focus of several dedicated studies (Shen et al. 2018; Bauer et al. 2021); here we only briefly remark on these objects. An analysis of the three HVS WD donors, assuming they were ejected following a D6-like scenario (given their $>1000\,\mathrm{km\,s^{-1}}$ velocities), suggested that two of the objects (D6-1 and D6-3) had to be massive ($\sim 1\,\mathrm{M_\odot}$), implying that the accretor would have been an even more massive CO WD in a nearly equal mass ratio binary (Bauer et al. 2021). The third HVS WD, D6-2, was found to be of lower mass, $\sim 0.4\,\mathrm{M_\odot}$, with looser mass constraints on its accretor. As discussed by Shen et al. (2018), D6-2 and D6-3 have radial velocities consistent with being $<100\,\mathrm{km\,s^{-1}}$, casting doubt on the interpretation of these stars as HVS stars. Furthermore, only one of the three WDs of Shen et al. (2018), D6-2, is considered to have highly significant parallax by Scholz (2018b), serving as a reliable extreme tangential velocity candidate, and even that one can be considered a doubtful high-speed candidate because of its relatively poor astrometric quality parameters (Scholz 2018b).

4.3.2 Additional candidates

Given our very high velocity cut for the sub-MS candidates, all of the candidates in Table 4 have velocities comparable to or higher than the Galactic escape velocity, making them, or at least most of them, less likely to be tail high-velocity halo objects (but, again, with the caveat of velocity measurement uncertainties), and these are therefore prime candidates for follow-up studies.

5 SEARCH FOR POSSIBLE WD–SUPERNOVA REMNANT ASSOCIATION

Some of the possible origins of HVS WDs are ejections following SN explosions. Such SNe leave SN remnants, that might be observable thousands of years after the explosion. It is therefore possible that some of our hyper-runaway WD candidates might be kinematically related to some SNR. Such possibility was recently explored by searching for WDs close to SNRs. Chandra et al. (2022) studied a SNR proposed to be the counterpart of LP 398-9 (D6-2). Shields et al. (2022) made a deep search for HVS WDs near SNR 1006, with null results. Here we search for all known SNRs whose positions could be consistent with the past propagation of WD HVSs. In order to investigate this possible link, we trace back the coordinates of fast-moving WDs from Table 1 and find the distances between these positions and locations of SNRs from the catalogue of Green (2019), Green (2009). Mathematically our procedure is as follows. The historical positions of a WD can be written as:

$$\alpha(t) = \alpha - \mu_\alpha t, \tag{4}$$

and

$$\delta(t) = \delta - \mu_\delta t, \tag{5}$$

where α, δ are the present-day right ascension and declination. Here, we do not take into account the Galactic gravitational potential because SNR are short-lived structures with ages rarely exceeding 10–20 kyr. Moreover, all the WDs in our selection are fast-moving objects which are not much affected by Galactic gravitational potential on even Myr time-scales.

The current distance between the SNR and the WD can be computed as:

$$D = \sqrt{(\alpha_{\rm SNR} - \alpha)^2 + (\delta_{\rm SNR} - \delta)^2}. \tag{6}$$

Then we introduce two vectors $\vec{p}$ and $\vec{\mu}$. The vector p can be written as:

$$\vec{p} = \begin{cases} (\alpha_{\rm SNR} - \alpha)/D \\ (\delta_{\rm SNR} - \delta)/D, \end{cases} \tag{7}$$

and the vector μ is a unit vector pointing in direction of the proper motion. The minimal distance between the WD path on the sky and the SNR can be computed as a vector product of $\vec{p}$ and $\vec{\mu}$:

$$d = D(p_\alpha \mu_\delta - \mu_\alpha p_\delta). \tag{8}$$

We assume that the SNR and the WD are related if $D < S_{\rm SNR}$ or $d < S_{\rm SNR}$ where $S_{\rm SNR}$ is the SNR size as provided by Green (2019). We additionally introduce the following constrains: (1) The WD should be moving away from the SNR, i.e. D is expect to grow with time, (2) the time necessary for the WD to reach its current position with respect to the SNR should be shorter than 100 kyr. With these constraints only WD *Gaia* DR3 5863122429179888000 could originate from a few SNRs, see Table 7. It happens because this WD is located close to the Galactic plane and move along the plane. Among SNR candidates only G309.8+00.0 and G310.8-00.4 seem plausible because they are shell SNR without any clear age estimate. Also, *Gaia* DR3 5863122429179888000 has a parallax of 13.23 mas which means that it is located at a distance of ≈75 pc from the Sun, while the distance of G310.8-00.4 is estimated to be 5 kpc. Two other candidates are not plausible because G308.8-00.1 seems to be associated with the radio pulsar PSR J1341-6220, while G315.4-02.3 is young (≈2000 yr) and located at a distance ≈2 kpc.

6 DISCUSSION

6.1 Possible origins of hyper-runaways and HVS WDs

As discussed above, we identify several unbound HVS WDs, which likely require significant velocity kicks, and about twenty HVS WDs and peculiar objects with velocities approaching the Galactic escape velocity. These identifications are very good candidates for WDs which experienced significant velocity kicks (even if formed in the halo). We also identified additional several tens of potential hyper-runaway WDs with lower velocities, which could also arise from such processes but might, instead, belong to the tail of non-kicked halo WDs.

We summarized all the scenarios leading to hyper-runaway WD formation in Table 8 together with the velocities of produced

Table 8. Summary of different scenarios which could lead to ejection of hyper-runaway WDs (or their immediate progenitors) together with their expected rates and features.

Scenario	SNe I type	Speed of ejected WD km s^{-1}	Features	Rate SNe Ia rate
Double degenerate dynamical detonation (D6)	Ia	>1000		1.0
Hybrid-WD reverse detonation	Ia	1000–1500	Heated and slightly polluted WD	0.01
Failed detonation/weak deflagration model	Iax	100–500	Hot, massive, polluted WD	0.2-0.5
Single-degenerate double-detonation	faint Ia	<600	sdB/sdO star is ejected	
Dynamical ejection in dense collisional enviroments	No SNRe	<400		
Binary/triple disruption by massibe black hole in Galactic centre	No SNRe	bound and unbound	Trajectory leads to Galactic centre	0.3 per year
Stripped stars from inspiralling galaxies	No SNRe	bound and unbound	Related to stellar streams	
Natal kick in a binary with neutron stars	No SNRe	<400	Tight NS-WD binary	

remnants and their important features. We will briefly go through all of these scenarios and explain if they are compatible with the observations.

6.2 Velocity kicks from SN explosions

6.2.1 Double-degenerate dynamical detonations and ejection of WDs

As suggested by Guillochon et al. (2010), Fink et al. (2010), two CO WDs with helium envelope are driven to each other by emission of gravitational radiation. At some point, after Roche overflow is initiated, the accretor experience thermonuclear detonation which causes secondary detonation inside the CO core of the accreator. The donor WD survives the SN Ia event and receives a large speed comparable to 1000–1500 km s^{-1}.

D6-1–D6-3, the only identified candidates with >1000 km s^{-1} were suggested to originate from this scenario (Shen et al. 2018; Bauer et al. 2021). However, the velocity of the best astrometric candidate, D6-2 (and potentially also D6-1 and D6-3, if they lie on the lowest velocity regime of the measurement uncertainty) could also be explained by a very different scenario such as the reverse detonation scenario mentioned above (Pakmor et al. 2021) and further discussed below, rather than the D6 scenario. Finally, even assuming all three HVS WDs are related to the D6 scenario, the non-detection of others in our and previous studies suggests that their ejection rate is at least two orders of magnitudes less than the inferred SN Ia rate (Shen et al. 2018). Furthermore, in our whole sample, we find only these three candidates to have estimated velocities exceeding 1000 km s^{-1}. Even accounting for the 95 per cent uncertainty intervals we calculated, only seven more candidates could have velocities exceeding 1000 km s^{-1}. In other words, even accounting for unlikely (but still possible) very large measurement errors, the overall number of extreme HVSs from a D6-like scenario are very small, compared to the type Ia SN rate expectations. Thus, this scenario is unlike to be responsible for all SN Ia events.

6.2.2 Hybrid-WD reverse detonation and ejection of WDs

In alternative scenario suggested by Pakmor et al. (2021), the first detonation in the accretor. He shell does not trigger the secondary detonation in the core, but instead the burning front propagates back to donor hybrid HeCO WD and its core detonates. Thus, in this scenario the donor is disrupted and accretor receives a large speed. The expected rate is around 1 per cent of all SNe Ia. In term of rates, this scenario could therefore potentially explain all the observed >1000 km s^{-1} HVS WDs, and be consistent with such a small number of identified HVS WDs. As discussed above, the low radial velocity of these objects raises concern regarding the reliability of the extreme velocity measurements. However, taken at face value, the reverse detonation is consistent with D6-2 velocity but at most marginally with the higher velocities of D6-1 and D6-3.

6.2.3 Failed-detonation/weak-deflagration model for Iax SNe and ejection of polluted WDs

As suggested by Jordan et al. (2012), an ignition of nuclear burning might not lead to a full detonation, but it could leave most of the WD intact. This event is seen as faint peculiar SNe Iax and could occur in 20–50 per cent of SNe Ia cases.

A number of a few up to a few tens of hyper-runaway WDs (possibly polluted or extremely hot WDs which would likely be observed as peculiar objects) would be comparable to the number of identified HVS WD candidates reported here and their origins could therefore be consistent with type Iax SNe.

6.2.4 Single-degenerate double-detonation models for faint Ia SNe and ejection of sdB/sdO stars

As suggested by Woosley et al. (1986), a massive WD accretes material from He-rich stellar companion. This companion becomes an sdB or sdO star. The accretor eventually accumulates enough mass to trigger explosion of the CO core which unbinds the companion. Our potential finding of tens such candidates, if verified as hyper-runaway sdB/O stars, could then be more consistent with the theoretical estimates of Neunteufel et al. (2022).

6.3 Dynamical ejections

6.3.1 Binary disruption following core-collapse supernova explosion

Some WDs can be formed as a result of binary disruption where the primary evolves off the MS and explodes as a core-collapse supernova. The secondary turns into a runaway star which eventually turns into a runaway WD. The formation of runaway and hyper-runaway stars via binary disruption following core-collapse supernova explosion was studied by Blaauw (1961), Tauris & Takens (1998), Portegies Zwart (2000), Tauris (2015), Evans, Renzo & Rossi (2020). In particular, Tauris (2015) found that standard binary stellar evolution could lead to ejection of stars with speeds above $v > 400$ km s^{-1}. However, the number of ejected stars with these velocities is not sufficient to explain hyper-runaway stars seen in our Galaxy (Evans et al. 2020). The number of hyper-runaway

stars produced via this channel are very sensitive to the common-envelope parameter α and the natal kick velocity distribution and could be increased if these two parameters are tuned. The rate of hyper-runaway WD formation via this channel was not studied in the literature, but at best it could give <2 per cent of all type-II SNe.

6.3.2 *Dynamical ejections in dense collisional environments*

It was suggested that close encounters between binaries and other stars/binaries in clusters could give rise to energy and momentum exchange leading to the ejection of runaway stars (Leonard & Duncan 1990; Perets & Šubr 2012; Oh & Kroupa 2016). Such stars, once they evolve, could later become WDs. However, the ejection velocities are of the order of the orbital velocities of the binary components participating in the encounter, which are typically limited (e.g. Leonard & Duncan 1990 obtained at most $\sim$200 km s^{-1}). One of us Perets & Šubr (2012) have shown in a detailed study of young clusters that the resulting runaway stars are typically ejected at moderate velocities and that ejection of hyper-runaway stars with velocities exceeding 400 km s^{-1} is rare. Ejection of runaway binaries, likely required for the formation of most sdB stars, is at even lower velocities.

6.3.3 *Binary/triple disruptions by the massive black hole in the Galactic centre*

Binary disruption by a massive black hole was suggested to produce HVS stars (Hills 1988) ejected at hundreds of km s^{-1} and even higher velocities, and could be unbound from the Galaxy. Observations of such HVS stars (Brown et al. 2005; Edelmann et al. 2005; Brown 2015) constrain their total number to at most a few hundreds of B-stars observable in the Galactic halo. Though bound HVS stars could be more abundant (Perets et al. 2009; Generozov & Perets 2022) their numbers would also be limited. Evans, Marchetti & Rossi (2022b), Evans, Marchetti & Rossi (2022a) found no reliable HVS in *Gaia* DR2 and thus set an upper limit to 3×10^{-1} yr^{-1}. Nevertheless, bound HVS stars could evolve to become WDs and be accumulated over the lifetime of the Galaxy, contributing to the population of extreme velocity WDs. This can be better constrained by following the WD trajectories and check whether they could be consistent with a Galactic centre origin. This is beyond the scope of this work but can be explored in later studies. While this mechanism can eject binary HVSs, it is less likely to do so, and therefore less likely to eject interacting binaries that might form sdB/O stars (Perets 2009a,b).

6.4 Stripped stars from inspiraling galaxies

Abadi, Navarro & Steinmetz (2009), Piffl, Williams & Steinmetz (2011) suggested that some HVS stars in the halo could also originate from stars stripped from a current or a past inspiraling galaxy. Such stars might be younger than the halo stellar population, and therefore could masquerade as disc stars ejected at high velocities. This would likely lead to a positional over density and velocity correlations of HVS stars in the sky. Excluding this possibility requires a more detailed study of the distribution of HVS stars across the sky, which is beyond the scope of the current study.

6.5 Natal kicks in binary NS – WD systems and the ejection of a NS-WD binary

Some of the systems summarized in Tables 1 and 4 showing velocities around 500 km s^{-1} could potentially be binaries with invisible NS component. For example, Heber (2009) discussed that there might exist a hidden population of massive compact companions (NSs or BHs) to sdB stars. Some NSs are known to receive natal kicks with amplitudes exceeding 600–800 km s^{-1} (Lyne & Lorimer 1994). If the system was compact before the SN explosion, or the natal kick was orientated favourably, the binary could survive a SN explosion and receive a significant centre-of-mass velocity.

In a recent work, we modelled different formation channels for NS-WD binaries (Toonen et al. 2018). We found that natal kick in the form suggested by Verbunt et al. (2017) could produce a small fraction of NS-WD binaries moving with speeds around 350–400 km s^{-1}. In this scenario, the NS could be too old to be seen as a radio pulsar. Even if the NS is still active as a radio pulsar, its radio beams could miss the Earth for the majority of these objects. NSs are typically very weak optical sources and not expected to be detected by *Gaia*. However, this hidden NS could be discovered in a series of WD spectral observations because the spectral lines will shift due to the orbital motion of the binary component.

The maximum systemic velocity which is reached by a NS-WD binary is very sensitive to the natal kick model and the properties of the common-envelope evolution (Toonen et al. 2018). Thus, detailed studies of these binaries could help to constrain both these aspects, but generally, this channel could lead to the production of hyper-runaway NS-WD binaries, though likely at the lower velocity regime we considered (around 400 km $^{-1}$). A detailed population synthesis is required to estimate the number of HVS WDs with invisible NS which could be seen in the *Gaia* survey.

7 CONCLUSIONS

In this work, we have analysed the *Gaia* DR3 catalogue to search for candidate hyper-runaway and HVS WDs and peculiar objects that could have been ejected at high velocities due to thermonuclear type Ia/Iax SNe or rare dynamical encounters. We identified most of the previously studied candidates (beside a few which had too large measurement uncertainties to pass our quality threshold), and found 46 of *n*ew WD and other non-MS peculiar HVS candidates (below the MS and above the WD region in the HR diagram). Our new candidates include 4 of highly likely unbound HVS WDs and sub-MS candidates and additional 42 of possible unbound HVSs (with velocities comparable to the escape velocity from the Galaxy). Among them, we identified 25 of hyper-runaway WDs. We determined the ages of several of these and exclude a halo origin for 5 (HVWDC 4, 7, 8, 11, 24), making them good candidates for being ejected from the Galactic disc through SNe/encounters. Most of the other WD candidates could also originate from the disc, but we cannot exclude a halo origin.

Overall we find that the number of identified candidates and their velocity distributions could be consistent with the expected contributions from type Iax SNe and reverse detonation of hybrid SNe, but likely rules out the double-detonation D6-model as a main contributor to the origin of normal type Ia SNe. Double-detonation in He-rich single-degenerate models may provide a non-negligible contribution to the origin of sdB/O runaways.

We also searched for HVS WDs with past trajectories crossing known SNe remnants, but found only one potential candidate, which might also be a chance coincidence. The lack of more candidates also disfavours the possibility that most type Ia SNe give rise to HVS WDs, as expected in the D6 scenario. We encourage follow-up studies of the identified candidates in order to better characterize their velocities and physical properties, which could then provide important constraints on the physical mechanisms for hyper-runaway ejections, and in particular the origins of type Ia/Iax SNe.

ACKNOWLEDGEMENTS

The work of API was supported by STFC grant number ST/W000873/1. HBP acknowledges support for this project from the European Union's Horizon 2020 research and innovation program under grant agreement number 865932-ERC-SNeX. The research of NH is supported by a Benoziyo prize postdoctoral fellowship. We thank anonymous referee, J.J. Hermes, B. Gänsicke, S.W. Jha, and R. Raddi for useful suggestions which helped us to significantly improve the manuscript.

This research has made use of the SIMBAD data base, operated at CDS, Strasbourg, France.

This work has made use of data from the European Space Agency (ESA) mission *Gaia* (https://www.cosmos.esa.int/gaia), processed by the *Gaia* Data Processing and Analysis Consortium (DPAC, https://www.cosmos.esa.int/web/gaia/dpac/consortium). Funding for the DPAC has been provided by national institutions, in particular the institutions participating in the *Gaia* Multilateral Agreement.

DATA AVAILABILITY

This work is based on publicly available data from the *Gaia* archive (see Appendix A for the ADQL query).

REFERENCES

Abadi M. G., Navarro J. F., Steinmetz M., 2009, ApJ, 691, L63
Arzoumanian Z., Chernoff D. F., Cordes J. M., 2002, ApJ, 568, 289
Bailer-Jones C. A. L., 2015, PASP, 127, 994
Bauer E. B., Chandra V., Shen K. J., Hermes J. J., 2021, ApJ, 923, L34
Bédard A., Bergeron P., Brassard P., Fontaine G., 2020, ApJ, 901, 93
Bildsten L., Shen K. J., Weinberg N. N., Nelemans G., 2007, ApJ, 662, L95
Blaauw A., 1961, Bull. Astron. Inst. Neth., 15, 265
Brandt N., Podsiadlowski P., 1995, MNRAS, 274, 461
Brown W. R., 2015, ARA&A, 53, 15
Brown W. R., Geller M. J., Kenyon S. J., Kurtz M. J., 2005, ApJ, 622, L33
Brown W. R., Beers T. C., Wilhelm R., Allende Prieto C., Geller M. J., Kenyon S. J., Kurtz M. J., 2008, AJ, 135, 564
Brown W. R., Kilic M., Allende Prieto C., Gianninas A., Kenyon S. J., 2013, ApJ, 769, 66
Capitanio L., Lallement R., Vergely J. L., Elyajouri M., Monreal-Ibero A., 2017, A&A, 606, A65
Casagrande L. et al., 2016, MNRAS, 455, 987
Chandra V. et al., 2022, MNRAS, 512, 6122
Choi J., Dotter A., Conroy C., Cantiello M., Paxton B., Johnson B. D., 2016, ApJ, 823, 102
Edelmann H., Napiwotzki R., Heber U., Christlieb N., Reimers D., 2005, ApJ, 634, L181
Eisenstein D. J. et al., 2006, ApJS, 167, 40
El-Badry K., Rix H.-W., 2018, MNRAS, 480, 4884
Eldridge J. J., Langer N., Tout C. A., 2011, MNRAS, 414, 3501
Evans F. A., Renzo M., Rossi E. M., 2020, MNRAS, 497, 5344
Evans F. A., Marchetti T., Rossi E. M., 2022a, MNRAS, 517, 3469
Evans F. A., Marchetti T., Rossi E. M., 2022b, MNRAS, 512, 2350
Fabricius C. et al., 2021, A&A, 649, A5
Fink M., Röpke F. K., Hillebrandt W., Seitenzahl I. R., Sim S. A., Kromer M., 2010, A&A, 514, A53
Foley R. J. et al., 2013, ApJ, 767, 57
Gaia Collaboration, 2016, A&A, 595, A1
Gaia Collaboration, 2022, preprint (arXiv:2208.00211)
Gänsicke B. T., Koester D., Raddi R., Toloza O., Kepler S. O., 2020, MNRAS, 496, 4079
Geier S. et al., 2015, Science, 347, 1126
Geier S., Østensen R. H., Nemeth P., Gentile Fusillo N. P., Gänsicke B. T., Telting J. H., Green E. M., Schaffenroth J., 2017, A&A, 600, A50
Generozov A., Perets H. B., 2022, MNRAS, 513, 4257
Gentile Fusillo N. P. et al., 2019, MNRAS, 482, 4570
Gentile Fusillo N. P. et al., 2021, MNRAS, 508, 3877
Green D. A., 2009, Bull. Astron. Soc. India, 37, 45
Green D. A., 2019, JA&A, 40, 36
Green R. F., Schmidt M., Liebert J., 1986, ApJS, 61, 305
Greenstein J. L., 1969, ApJ, 158, 281
Guillochon J., Dan M., Ramirez-Ruiz E., Rosswog S., 2010, ApJ, 709, L64
Heber U., 2009, ARA&A, 47, 211
Hermes J. J., Putterman O., Hollands M. A., Wilson D. J., Swan A., Raddi R., Shen K. J., Gänsicke B. T., 2021, ApJ, 914, L3
Hills J. G., 1988, Nature, 331, 687
Hirsch H. A., Heber U., O'Toole S. J., Bresolin F., 2005, A&A, 444, L61
Hoogerwerf R., de Bruijne J. H. J., de Zeeuw P. T., 2001, A&A, 365, 49
Igoshev A. P., 2020, MNRAS, 494, 3663
Igoshev A., Verbunt F., Cator E., 2016, A&A, 591, A123
Igoshev A. P., Chruslinska M., Dorozsmai A., Toonen S., 2021, MNRAS, 508, 3345
Jofré P., Weiss A., 2011, A&A, 533, A59
Jordan, George C. I., Perets H. B., Fisher R. T., van Rossum D. R., 2012, ApJ, 761, L23
Kawka A., Vennes S., Ferrario L., 2020, MNRAS, 491, L40
Kepler S. O. et al., 2015, MNRAS, 446, 4078
Kepler S. O., Koester D., Ourique G., 2016, Science, 352, 67
Kilic M. et al., 2006, AJ, 131, 582
Kilic M., Bergeron P., Dame K., Hambly N. C., Rowell N., Crawford C. L., 2019, MNRAS, 482, 965
Kromer M. et al., 2013, MNRAS, 429, 2287
Lamontagne R., Demers S., Wesemael F., Fontaine G., Irwin M. J., 2000, AJ, 119, 241
Leonard P. J. T., Duncan M. J., 1990, AJ, 99, 608
Lépine S., Shara M. M., 2005, AJ, 129, 1483
Li W. et al., 2011, MNRAS, 412, 1441
Lindegren L. et al., 2021, A&A, 649, A4
Liu Z.-W., Röpke F. K., Zeng Y., Heger A., 2021, A&A, 654, A103
Lorimer D. R. et al., 2006, MNRAS, 372, 777
Lutz T. E., Kelker D. H., 1973, PASP, 85, 573
Lyne A. G., Lorimer D. R., 1994, Nature, 369, 127
Lynn B. B. et al., 2004, MNRAS, 353, 633
Marchetti T., 2021, MNRAS, 503, 1374
Marchetti T., Rossi E. M., Brown A. G. A., 2019, MNRAS, 490, 157
Meng X.-C., Luo Y.-P., 2021, MNRAS, 507, 4603
Monari G. et al., 2018, A&A, 616, L9
Napiwotzki R., 2008, in Heber U., Jeffery C. S., Napiwotzki R., eds, ASP Conf. Ser. Vol. 392, Hot Subdwarf Stars and Related Objects. Astron. Soc. Pac., San Francisco, p. 139
Neunteufel P., Preece H., Kruckow M., Geier S., Hamers A. S., Justham S., Podsiadlowski P., 2022, A&A, 663, A91
O'Donoghue D., Kilkenny D., Koen C., Hambly N., MacGillivray H., Stobie R. S., 2013, MNRAS, 431, 240
Oh S., Kroupa P., 2016, A&A, 590, A107
Pakmor R., Zenati Y., Perets H. B., Toonen S., 2021, MNRAS, 503, 4734
Perets H. B., 2009a, ApJ, 690, 795
Perets H. B., 2009b, ApJ, 698, 1330
Perets H. B., Šubr L., 2012, ApJ, 751, 133
Perets H. B., Wu X., Zhao H. S., Famaey B., Gentile G., Alexander T., 2009, ApJ, 697, 2096
Perets H. B. et al., 2010, Nature, 465, 322
Piffl T., Williams M., Steinmetz M., 2011, A&A, 535, A70
Portegies Zwart S. F., 2000, ApJ, 544, 437
Raddi R., Hollands M. A., Gänsicke B. T., Townsley D. M., Hermes J. J., Gentile Fusillo N. P., Koester D., 2018a, MNRAS, 479, L96
Raddi R., Hollands M. A., Koester D., Gänsicke B. T., Gentile Fusillo N. P., Hermes J. J., Townsley D. M., 2018b, ApJ, 858, 3
Raddi R. et al., 2019, MNRAS, 489, 1489
Reid M. J. et al., 2014, ApJ, 783, 130
Renzo M. et al., 2019, A&A, 624, A66
Repetto S., Davies M. B., Sigurdsson S., 2012, MNRAS, 425, 2799
Repetto S., Igoshev A. P., Nelemans G., 2017, MNRAS, 467, 298

Ruffini N. J., Casey A. R., 2019, MNRAS, 489, 420
Sayres C., Subasavage J. P., Bergeron P., Dufour P., Davenport J. R. A., AlSayyad Y., Tofflemire B. M., 2012, AJ, 143, 103
Scholz R.-D., 2018a, Res. Notes Am. Astron. Soc., 2, 211
Scholz R.-D., 2018b, Res. Notes Am. Astron. Soc., 2, 211
Schönrich R., Binney J., Dehnen W., 2010, MNRAS, 403, 1829
Shen K. J., Kasen D., Miles B. J., Townsley D. M., 2018, ApJ, 854, 52
Shen K. J. et al., 2018, ApJ, 865, 15
Shields J. V. et al., 2022, ApJ, 933, L31
Smith L. C. et al., 2018, MNRAS, 474, 1826
Tauris T. M., 2015, MNRAS, 448, L6
Tauris T. M., Takens R. J., 1998, A&A, 330, 1047
Tillich A. et al., 2011, A&A, 527, A137
Toonen S., Perets H. B., Igoshev A. P., Michaely E., Zenati Y., 2018, A&A, 619, A53
Vennes S., Nemeth P., Kawka A., Thorstensen J. R., Khalack V., Ferrario L., Alper E. H., 2017, Science, 357, 680
Verbiest J. P. W., Weisberg J. M., Chael A. A., Lee K. J., Lorimer D. R., 2012, ApJ, 755, 39
Verbunt F., Igoshev A., Cator E., 2017, A&A, 608, A57
Wenger M. et al., 2000, A&AS, 143, 9
Woosley S. E., Taam R. E., Weaver T. A., 1986, ApJ, 301, 601
Zenati Y., Toonen S., Perets H. B., 2019, MNRAS, 482, 1135
Zenati Y., Perets H. B., Dessart L., Jacobson-Gal'an W. V., Toonen S., Rest A., 2022, preprint (arXiv:2207.13110)
Ziegerer E., Heber U., Geier S., Irrgang A., Kupfer T., Fürst F., Schaffenroth J., 2017, A&A, 601, A58

APPENDIX A: ADQL REQUEST

Our basic request is:

```
  select top 1000 *, abs(pm)/parallax as v
  from gaiadr3.gaia_source
  where parallax_over_error > 4 and paral-
lax > 0.25
  and RUWE < 1.4 and IPD_FRAC_MULTI_PEAK < = 2
  and IPD_GOF_HARMONIC_AMPLITUDE < 0.1
  and ASTROMETRIC_SIGMA5D_MAX < 1.5
  and PHOT_G_MEAN_MAG-5*log10(1000.0/parallax)
  +5 > 6 + 5 * bp_rp
  order by v DESC
```

Our relaxed request is:

```
  select top 1000 *, abs(pm)/parallax as v
  from gaiadr3.gaia_source
  where parallax_over_error > 4
  and parallax > 0.25
  and RUWE < 1.4
  and IPD_FRAC_MULTI_PEAK < = 2
  and IPD_GOF_HARMONIC_AMPLITUDE < 0.1
  and ASTROMETRIC_SIGMA5D_MAX < 1.5
  and PHOT_G_MEAN_MAG
  - 5*log10(1000.0/parallax)+5 > 0.66 + 6.67
* bp_rp
  order by v DESC
```

APPENDIX B: A POSTERIOR ESTIMATE FOR THE TRANSVERSAL VELOCITY AND CREDIBLE INTERVALS

The nominal transversal velocity is computed as:

$$v_t[\mathrm{km\,s^{-1}}] = \frac{4.74\sqrt{\mu_\alpha^2+\mu_\delta^2}[\mathrm{mas\ yr^{-1}}]}{\varpi'[\mathrm{mas}]}. \tag{B1}$$

If we apply the error propagation technique to this equation we obtain:

$$\sigma_\mu = \sqrt{\frac{\mu_\alpha^2}{\mu_\alpha^2+\mu_\delta^2}\sigma_{\mu,\alpha}^2 + \frac{\mu_\delta^2}{\mu_\alpha^2+\mu_\delta^2}\sigma_{\mu,\delta}^2} \tag{B2}$$

$$\sigma_{vt} = v_t\sqrt{\frac{\sigma_\mu^2}{\mu^2}+\frac{\sigma_\varpi^2}{\varpi'^2}}. \tag{B3}$$

In many cases $\sigma_\mu/\mu < 0.01$ while $\sigma_\varpi/\varpi' \approx 0.2$, thus the parallax uncertainty is the leading contribution to the total velocity uncertainty. The main problem of this error estimate equation (B3) is that it is symmetric around the nominal velocity while symmetric errors of parallax measurement translate to skewed error distribution for distance. This problem is known as the Lutz–Kelker bias (Lutz & Kelker 1973) for survey and was addressed in multiple earlier works, see e.g. Bailer-Jones (2015), Igoshev et al. (2016).

This problem can be solved if we write a Bayesian posterior for transversal velocity and make all our priors explicit. In our approach

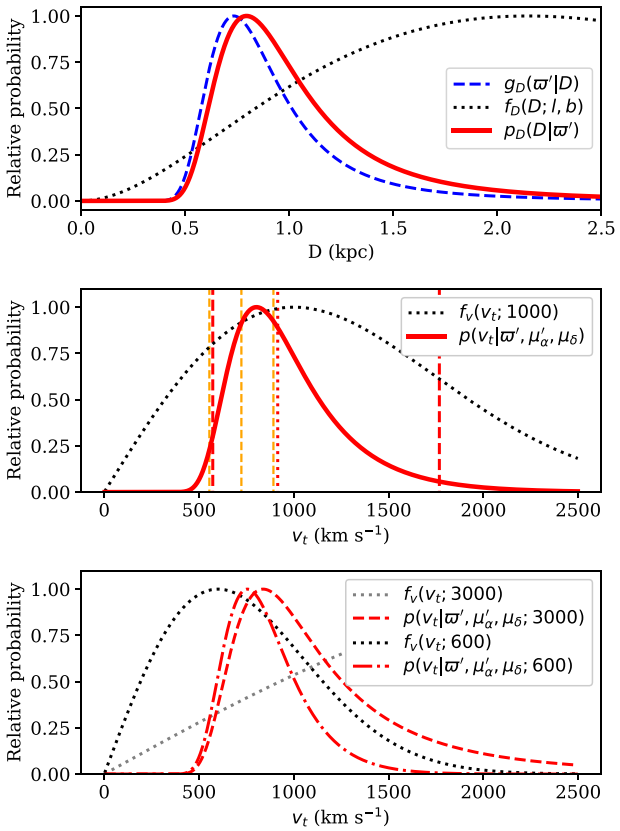

Figure B1. Posterior distribution for distance (top panel) and for tangential velocity (two lower panels) for *Gaia* DR3 5703888058542880896. Dotted-black line at the top panel shows the Galactic prior in the direction of the source; dashed-blue line shows conditional probability for parallax given distance and solid red curve shows the posterior distribution. Lower panels show the posterior distribution for tangential velocities assuming that proper motion is measured exactly. In the middle panel, yellow lines show the nominal velocity (dashed line) and 68 per cent confidence interval computed using the error propagation technique. Red lines show the median of the posterior distribution (dotted line) and 95 per cent credential interval. In the lower panel, grey and black dotted lines show priors for velocity distribution with $\sigma = 3000\,\mathrm{km\,s^{-1}}$ and $\sigma = 600\,\mathrm{km\,s^{-1}}$, respectively. Red lines show posterior for the case when it is assumed $\sigma = 3000\,\mathrm{km\,s^{-1}}$ (dashed line) and $\sigma = 600\,\mathrm{km\,s^{-1}}$ (dot-and-dashed line) for the velocity prior.

we assume that proper motion is measured exactly, thus $\mu/\sigma_\mu \gg 1$ which is true for our high-speed objects. For example for *Gaia* DR3 5703888058542880896, $\mu/\sigma_\mu \approx 500$.

Even though our proper motion measurements are so precise, we need to choose a prior for the velocity distribution to specify our expectations about the velocity. It is useful to show that uniform prior is relatively bad assumption. Let us for a moment assume that $v_x \sim U(-v_{\max}, v_{\max})$. It means that transversal velocity $v_t = \sqrt{v_x^2 + v_y^2}$ is drawn from another distribution. In order to obtain a distribution for v_t, we transform to a polar coordinate system and integrate over angle θ:

$$p(v_t) = \int_0^{2\pi} U(v_t \sin\theta) U(v_t \cos\theta) v_t \mathrm{d}\theta, \tag{B4}$$

where $U(x)$ is the probability density function for uniform distribution. The result of this integration is counter-intuitive:

$$p(v_t) = \begin{cases} v_t/(4v_{\max}^2), & \text{if } |v_x| < v_{\max} \ \& \ |v_y| < v_{\max} \\ 0 & \text{otherwise.} \end{cases} \tag{B5}$$

It means that it is more probable for system to have v_t comparable to $v_{\max}$ than small some velocity. Also increasing $v_{\max}$ will lead to an increase in speed. Thus such a prior will not be useful. Instead, we introduce a prior in form of normal distribution for each velocity component:

$$v_\alpha = \frac{1}{\sqrt{2\pi}\sigma} \exp\left(-\frac{v^2}{2\sigma^2}\right). \tag{B6}$$

This prior has multiple great properties: (1) smaller velocities are more probable than larger velocities, (2) if σ is large in comparison to velocities under study, the prior becomes similar to uniform prior. The tangential velocity distribution is simply:

$$\begin{aligned} f_v(v_t) &= \int_0^{2\pi} \frac{v_t}{2\pi\sigma^2} \exp\left[-\frac{v^2\sin^2\theta}{2\sigma^2} - \frac{v^2\cos^2\theta}{2\sigma^2}\right] \mathrm{d}\theta \\ &= \frac{v_t}{\sigma^2} \exp\left[-\frac{v_t^2}{2\sigma^2}\right]. \end{aligned} \tag{B7}$$

Here, we replace the component of tangential velocity v_α, v_δ by using absolute value of the velocity v_t and polar angle such a way that:

$$v_\alpha = v_t \sin\theta, \tag{B8}$$

and

$$v_\delta = v_t \cos\theta. \tag{B9}$$

The joint probability to measure parallax ϖ', proper motions μ'_α and μ'_δ, tangential velocity v_t, polar angle θ, and distance D can be written as:

$$\begin{aligned} p(\varpi', \mu'_\alpha, \mu'_\delta, v_t, \theta, D) = g(\varpi'|D) f_D(D; l, b) g(\mu'_\alpha|v_t, \theta, D) \\ \times g(\mu'_\delta|v_t, \theta, D) f_v(v_t; \sigma), \end{aligned} \tag{B10}$$

where $g(\varpi'|D)$ is the conditional probability to measure parallax given the actual distance. It is written as the normal distribution:

$$g(\varpi'|D) = \frac{1}{\sqrt{2\pi}\sigma_\varpi} \exp\left[-\frac{(1/D - \varpi')^2}{2\sigma_\varpi^2}\right], \tag{B11}$$

where σ_ϖ is the uncertainty of parallax measurement. The function $f_D(D; l, b)$ is our Galactic prior for distances same as in Verbiest et al. (2012):

$$f_D(D; l, b) = D^2 R^{1.9} \exp\left[-\frac{|z(D,l,b)|}{h_z} - \frac{R(D,l,b)}{H_R}\right]. \tag{B12}$$

In this case, l and b are Galactic latitude and longitude, respectively. Since most star formation occurs in the thin disc, we assume that $h = 0.33$ kpc and $H_R = 1.7$ kpc using the values by Lorimer et al. (2006) found for young radio pulsars. The functions $g(\mu'_\alpha|v_t, \theta, D)$ and $g(\mu'_\delta|v_t, \theta, D)$ are conditional probabilities to measure respective component of the proper motion given transversal velocity, angle, and distance. These are represented by normal distribution in form:

$$\begin{aligned} &g(\mu'_\alpha|v_t, \theta, D) \\ &= \frac{1}{\sqrt{2\pi}\sigma_{\mu,\alpha}} \exp\left[-\frac{(\mu'_\alpha - v_t \sin\theta/(4.74D) - \Delta\mu_\alpha)^2}{2\sigma_{\mu,\alpha}^2}\right]. \end{aligned} \tag{B13}$$

In this equation, $\Delta\mu_\alpha$ is the correction for Galaxy rotation. In this work, we do not use these corrections to estimate the credible intervals because our sources are close to the Sun and Galactic rotation does not change their velocities significantly.

In order to get rid of unknown D and θ we integrate over these quantities. The integral over θ is hard to compute analytically because it involves terms in form $\propto \exp(-(vt^2 \sin^2\theta)$. Instead we deal with terms $g(\mu'_\alpha|v_t, \theta, D) g(\mu'_\delta|v_t, \theta, D)$ as the following. The maximum of this function is located approximately at:

$$\tan(\theta + \pi) = \frac{(\mu'_\alpha - \Delta\mu_\alpha)}{(\mu'_\delta - \Delta\mu_\delta)}. \tag{B14}$$

Sometimes it is shifted by π from this location that is why we numerically check both points. It is located exactly at this position if $\sigma_{\mu,\alpha} = \sigma_{\mu,\delta}$. Thus, we use the Nelder–Mead algorithm to iterate and find exact maximum of this function. Next, we iterate again looking for the situation when $g(\mu'_\alpha|v_t, \theta, D) g(\mu'_\delta|v_t, \theta, D)$ decreased by two orders of magnitude. Thus, we end up with two angles θ_0 and θ_1. We integrate numerically between these two angles using 20 mesh points distributed uniformly. The result of this integration is numerical constant κ, which is unique for v_t and D combination.

Proceeding further, we could notice that in our case function $g(\mu'_\alpha|v_t, \theta, D) g(\mu'_\delta|v_t, \theta, D) \approx 1$ only around value:

$$d_1 = \frac{v_t}{4.74\sqrt{(\mu'_\alpha - \Delta\mu_\alpha)^2 + (\mu'_\delta - \Delta\mu_\delta)^2}}. \tag{B15}$$

Basically, this is the distance which corresponds to proper motion μ if v_t is fixed. It happens because our errors for proper motion are tiny. Therefore, we can simply replace the integration over distance with posterior function at distance d_1:

$$p(\varpi', \mu'_\alpha, \mu'_\delta, v_t) = g(\varpi'|d_1) f_D(d_1; l, b) f_v(v_t; \sigma) \kappa. \tag{B16}$$

We show the posterior estimate for distance and transversal velocity of *Gaia* DR3 5703888058542880896 in Fig. B1. As it is clear from the figure, error propagation technique gives poor estimate for errors underestimating the size of high-velocity tail. In our calculations, we fix σ in the velocity prior at value $\sigma = 1000\,\mathrm{km\,s^{-1}}$ which is wide enough to cover all our velocity range. In Fig. B1, we also show the posterior distribution for two-velocity computed with prior $f_v(v_t; 3000)$ and $f_v(v_t\ ; 600)$. In the case of $\sigma = 3000\,\mathrm{km\,s^{-1}}$, the distribution becomes slightly wider. Respectively, in the case of $\sigma = 600\,\mathrm{km\,s^{-1}}$, the posterior velocity distribution shrinks.

This paper has been typeset from a TEX/LATEX file prepared by the author.